Journal of Medicinal Chemistry

Article

Acyl Ureas as Human Liver Glycogen Phosphorylase Inhibitors for the Treatment of Type 2 Diabetes

Thomas Klabunde, K. Ulrich Wendt, Dieter Kadereit, Volker Brachvogel, Hans-Jrg Burger, Andreas W. Herling, Nikos G. Oikonomakos, Magda N. Kosmopoulou, Dieter Schmoll, Edoardo Sarubbi, Erich von Roedern, Karl Schnafinger, and Elisabeth Defossa

J. Med. Chem., **2005**, 48 (20), 6178-6193• DOI: 10.1021/jm049034y • Publication Date (Web): 09 September 2005

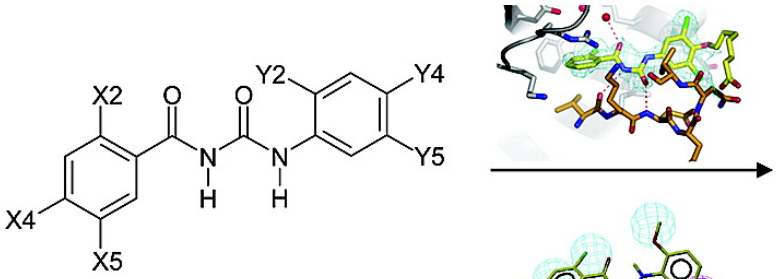

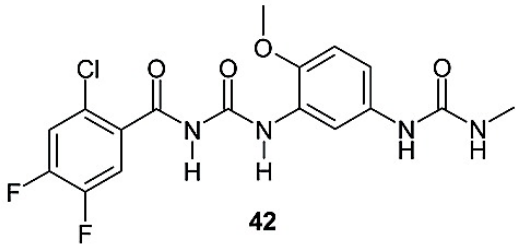

42

in vivo active compound

More About This Article

Additional resources and features associated with this article are available within the HTML version:

- Supporting Information
- Links to the 5 articles that cite this article, as of the time of this article download
- Access to high resolution figures
- Links to articles and content related to this article
- Copyright permission to reproduce figures and/or text from this article

Journal of Medicinal Chemistry is published by the American Chemical Society. 1155 Sixteenth Street N.W., Washington, DC 20036

Articles

Acyl Ureas as Human Liver Glycogen Phosphorylase Inhibitors for the Treatment of Type 2 Diabetes

Thomas Klabunde, K. Ulrich Wendt, Dieter Kadereit, Volker Brachvogel, Hans-Jörg Burger, Andreas W. Herling, Nikos G. Oikonomakos,† Magda N. Kosmopoulou,† Dieter Schmoll, Edoardo Sarubbi, Erich von Roedern, Karl Schönafinger, and Elisabeth Defossa*

Sanofi-Aventis Deutschland GmbH, Scientific and Medical Affairs, D-65926 Frankfurt am Main, Germany, and Institute of Organic and Pharmaceutical Chemistry, and Institute of Biological Research and Biotechnology, The National Hellenic Research Foundation, Athens 11635, Greece

Received November 30, 2004

Using a focused screening approach, acyl ureas have been discovered as a new class of inhibitors of human liver glycogen phosphorylase (hlGPa). The X-ray structure of screening hit **1** (IC_{50} = 2 μM) in a complex with rabbit muscle glycogen phosphorylase b reveals that **1** binds at the AMP site, the main allosteric effector site of the dimeric enzyme. A first cycle of chemical optimization supported by X-ray structural data yielded derivative **21**, which inhibited hlGPa with an IC_{50} of 23 ± 1 nM, but showed only moderate cellular activity in isolated rat hepatocytes (IC_{50} = 6.2 μM). Further optimization was guided by (i) a 3D pharmacophore model that was derived from a training set of 24 compounds and revealed the key chemical features for the biological activity and (ii) the 1.9 Å crystal structure of **21** in complex with hlGPa. A second set of compounds was synthesized and led to **42** with improved cellular activity (hlGPa IC_{50} = 53 ± 1 nM; hepatocyte IC_{50} = 380 nM). Administration of **42** to anaesthetized Wistar rats caused a significant reduction of the glucagon-induced hyperglycemic peak. These findings are consistent with the inhibition of hepatic glycogenolysis and support the use of acyl ureas for the treatment of type 2 diabetes.

Introduction

Type 2 diabetes or non-insulin-dependent diabetes mellitus is a severe and prevalent disease of arguably epidemic proportions in the industrialized world. The elevated blood glucose levels characteristic of this medical condition are in part caused by an increased hepatic glucose production and promote the risk of premature death due to cardiovascular complications.[1] Two metabolic pathways, glycogenolysis and gluconeogenesis, enable the liver to produce glucose.[2] The inhibition of glycogen breakdown as an antidiabetic strategy has recently attracted a lot of interest.[3] Glycogen phosphorylase (GP) is the rate-controlling enzyme of glycogen degradation. It catalyzes the phosphorolytic cleavage of α-1,4 glycosidic bonds in glycogen, yielding glucose-1-phosphate. The homodimeric GP is physiologically regulated through small molecule allosteric effectors as well as through phosphorylation at serine-14, resulting in a structural switch between active (R-state) and inactive (T-state) conformations.[4,5] Phosphorylation to the phosphorylase-a form (GPa) promotes the active R-state. The main allosteric effector site is located away from the active site (Figure 1) and is referred to as the AMP site. A second allosteric site, the i-site, binds purine-like compounds, such as caffeine and other nucleosides, and is of unkown physiological function. Inhibitors of hlGP have been found to bind to the active site,[6] the allosteric AMP site,[7−9] and the i-site.[10] Recently, a class of synthetic inhibitors was found to bind to a site at the dimer interface (Figure 1).[11−15]

Here we report a new class of GP inhibitors with an acyl urea scaffold readily amenable to parallel synthesis. X-ray crystallography studies demonstrate that the inhibitors bind to the allosteric AMP site. On the basis of these findings, rational design and parallel synthesis were used to develop an hlGP inhibitor with excellent in vivo activity.

Results and Discussion

Lead Finding. A novel class of glycogen phosphorylase inhibitors, exemplified by compound **1** (Scheme 1), was identified by focused screening. A set of 60 compounds that revealed pharmacophoric similarities to known glycogen phosphorylase inhibitors was selected for focused screening from the company's compound repository and was tested experimentally. Of this set, compound **1** showed activity in the hlGPa (IC_{50} = 2 μM) as well as in the rabbit muscle glycogen phosphorylase b (rabmGPb) enzyme assay (IC_{50} = 2.2 μM). Only moderate cellular activity was seen when tested in rat hepatocytes (IC_{50} = 80 μM). Subsequent biochemical characterization indicated that the inhibition of hlGPa by **1** is independent of the direction of the reaction (similar inhibition of glycogen breakdown and

* Corresponding author. Phone: +49-69-305-13078. Fax +49-69-331399. E-mail: elisabeth.defossa@sanofi-aventis.com.
† The National Hellenic Research Foundation.

10.1021/jm049034y CCC: $30.25
Published on Web 09/09/2005

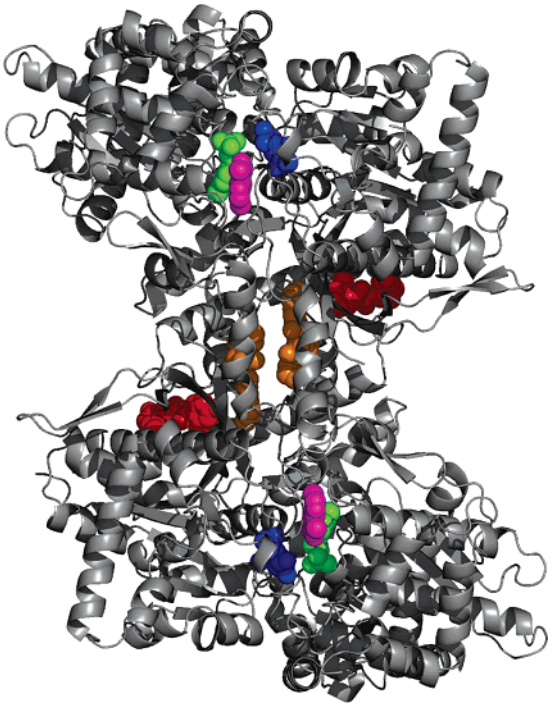

Figure 1. Active site and allosteric sites of dimeric hlGPa. The protein (coordinates from PDB entry 1L7X)[44] is shown as a ribbon diagram (gray). The different sites are highlighted through CPK models of the respective ligands in PDB entry 1L7X and the hlGP−**21** structure reported herein: pyridoxal phosphate (active site; green), *N*-acetyl-*β*-D-glucopyranosylamine (active site; blue), caffeine (i-site; magenta), CP-403700 (dimer interface; orange), and superimposed acyl urea inhibitor **21** (red), which binds at the AMP site (AMP not shown).

Scheme 1

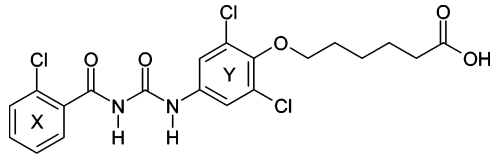

1

synthesis). Furthermore, the inhibition by **1** is competitive to adenosine monophosphate (AMP) and additive to glucose in both assay directions (data not shown).

Structure of Acyl Urea 1 in a Complex with Rabbit Muscle GPb. To identify the binding site of **1**, we determined the structure of the complex with rabmGPb at 2.3 Å resolution (Figure 2). The structure reveals that **1** binds to the allosteric AMP site of the enzyme, partially overlapping with the position of AMP as observed within the GP−AMP complex (PDB ID 1FA9).[4] Binding of compound **1** into the AMP site is consistent with the lower potency in the presence of elevated AMP concentration, as observed experimentally. **1** binds in a slightly twisted conformation that allows for the formation of an intramolecular hydrogen bond within the central acyl urea moiety. The benzoyl ring (X, Scheme 1) is buried in a narrow side pocket deep in the AMP site. The phenyl ring (Y, Scheme 1) points toward the entrance of the AMP site, and the aliphatic carboxylate side chain of **1** protrudes from this opening into the bulk solvent.

The inhibitor is located at the interface of the dimer forming the AMP site. The central acyl urea moiety hydrogen bonds with the carbonyl group of Val40′ (where the prime refers to residues from the symmetry-related subunit), the backbone amide group of Asp42′, and an ordered water molecule in the upper part of the AMP pocket (as indicated by red dashed lines in Figure 2). In addition, the 2-chloro-substituted benzoyl ring (X) shows π stacking and van der Waals interactions with side chains of Trp67, Arg193, Val40′, and Lys41′. The interactions of the phenyl ring (Y) are less prominent, involving van der Waals interactions of the 3,5-dichloro-substituted aromatic ring with side chains at the entrance of the cavity (e.g., Tyr75 and Asn44′) as well as a notable steric clash between one of the chlorines and the C_β of Tyr75.

Compound Synthesis and Optimization of hlGPa Enzyme Inhibitor Activity. Chemical variations at the benzoyl ring (X) and the phenyl ring (Y) of screening hit **1** were performed (i) to improve the biological activity of **1** and (ii) to derive detailed structure−activity relationship (SAR) information that would guide subsequent optimization cycles. The parallel synthesis efforts were guided by the molecular insights into the enzyme−inhibitor interaction gained from the structure of the complex of **1** with rabmGP: (1) At the benzoyl ring (X) we focused on sterically conservative substitutions in the ortho (X2) and para (X4) position. Positions X3 and X6 appeared unsuited for modification due to close contacts with the conserved residues Trp67 and Lys41′ (Figure 2). (2) At the phenyl ring (Y) we attempted to introduce sterically more demanding substituents at the ortho position to reach into the upper part of the AMP pocket (Y2), and we replaced the disordered aliphatic carboxylate side chain in the para position (Y4) with shorter charged and uncharged residues. (3) In addition, we probed the possibility to introduce additional hydrogen bonds with the side chains of Asp42′ and Asn44′ by introducing a hydroxy function in the meta position (Y5). (4) The chloro group in the meta position (Y3) of **1** was removed to avoid the apparent steric clash with the C_β atom of the conserved Tyr75.

The synthesis of acyl ureas is described in the literature by the reaction of isocyanates with amines or amides, as outlined in Scheme 2.[16−20] Benzoylphenyl ureas can be prepared by two different methods, either by using a benzoyl isocyanate moiety on the X-ring reacting with a substituted aniline (route A) or by using an isocyanate moiety on the Y-ring reacting with a substituted benzamide (route B).[21−24] Most compounds were prepared by route A, which is amenable to parallel and robotic synthesis. Only for compound **37** route B was chosen. The synthetic steps are shown in Scheme 2 and experimental details are given in the Experimental Section.

A set of 24 acyl urea derivatives was prepared (compounds **2**−**25**). All compounds were assessed for their ability to inhibit the hlGPa, and active compounds were subsequently tested in the rat hepatocyte assay (Table 1). The following SAR was observed for the enzyme inhibitory activity: X2 = Cl more active than (>) F; X4 = F > Cl > H; Y2 = Cl ~ OMe ~ OCF_3 > H; Y4 = COOH ~ tetrazole > SO_2NH_2 ~ COOMe. The comparison of phenolic acyl ureas (Y5 = OH) with carboxylic acid derivatives (Y4 = COOH) shows that the

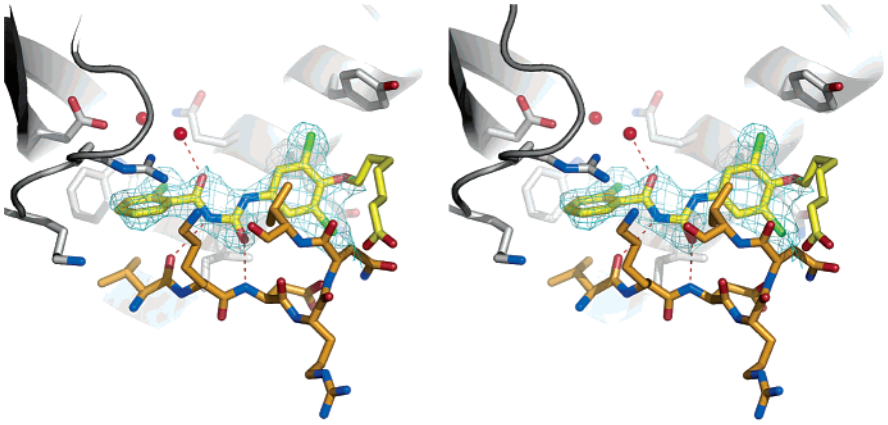

Figure 2. Stereoview of the binding mode of screening hit **1** at the allosteric AMP site of rabbit muscle glycogen phosphorylase b (rabmGPb). The AMP site resides at the dimer interface of rabmGPb. Monomer **1** is shown in gray and part of the "cap" region (Val40′, Lys41′ to Asn44′, Val45′) of monomer **2** is shown in orange. The scaffold of the bound inhibitor (yellow) is well defined in the $2F_o - F_c$ electron density (cyan; contour level at 1.0σ). The aliphatic carboxylate side chain is not covered by the electron density, indicating flexibility or disorder for this part of the inhibitor. The central acyl urea scaffold forms hydrogen bonds (red dashes) with the main chain of Val40′ (3.0 Å distance), Asp42′ (3.0 Å), and an ordered water molecule in the upper part of the AMP pocket (2.8 Å).

Scheme 2. Synthetic Routes for the Synthesis of Acyl Ureas

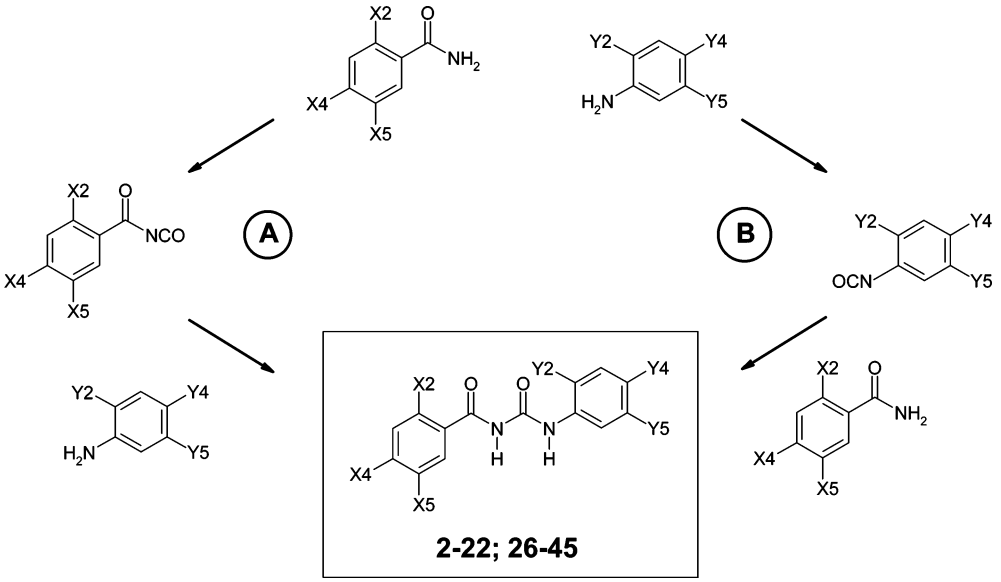

phenols are 10-fold more active (**3** vs **11** and **7** vs **21**). The most active phenol derivative **21** revealed a 100-fold improvement in enzymatic activity ($IC_{50} = 23 \pm 1$ nM), when compared to the original screening hit **1** ($IC_{50} = 2$ μM). Regarding the biological activity in the rat hepatocyte assay, compound **21** was significantly less active ($IC_{50} = 6.2$ μM, see Table 1). For the carboxylic acid derivatives, X4 = F enhanced the cellular activity (**2** vs **8** and **3** vs **7**), a finding that is not seen for the phenol derivative **21** (**21** vs **11**).

Although we did not have a clear rationale for the significant activity drop observed in the rat hepatocyte assay, we suspected that metabolic instability—especially for the phenolic derivatives of the series—might be the main cause. Prior to the next optimization cycle, a 3D pharmacophore model was generated in order to identify chemical features that mediated the good activity of compound **21** in the enzymatic assay. We intended to either maintain these chemical groups or to replace them by groups with corresponding pharmacophoric features. We also determined the structure of compound **21** in complex with hlGPa.

3D Pharmacophore Model and Structure of Acyl Urea 21 in Complex with hlGPa. The 3D pharmacophore hypothesis was generated within Catalyst using the molecules **2**–**25** as training set (Table 1). The resulting pharmacophore model contains five features, including one hydrogen-bond acceptor (HBA), one hydrogen-bond donor (HBD), and three hydrophobic features (HYD). It provides direct information on the spatial arrangement of these chemical features required for enzyme inhibitory activity. Mapping of the most active compound **21** ($IC_{50} = 23 \pm 1$ nM) onto the pharmacophore model is depicted in Figure 3a. Besides the acyl urea scaffold, the hydrophobic methoxy substituent (Y2), the phenolic hydroxyl substituent (Y5), as well as the benzoylic chlorine substituent (X2) appear to be key contributors to the enzyme inhibitory activity of this series. The activities estimated on the basis of the fit onto the pharmacophore hypothesis are in good agreement with the experimental values (correlation *R*

Table 1. Experimental Activities from the hlGPa Enzyme and the Cellular Hepatocyte Assay

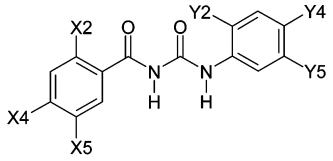

2-22; 26-45

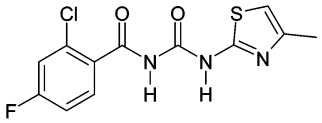

23

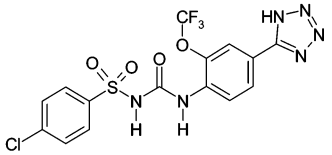

24

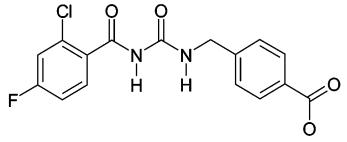

25

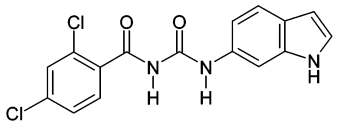

44

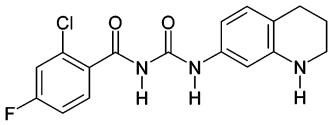

45

compd	X2	X4	X5	Y2	Y4	Y5	IC_{50}[a,b] enzyme (nM)	IC_{50}[a,b] hepatocyte (μM)
2	Cl	H	H	Cl	COOH	H	940	19
3	Cl	H	H	OMe	COOH	H	850	28
4	Cl	Cl	H	OMe	COOH	H	510	23
5	Cl	Cl	H	Cl	COOH	H	420	9
6	F	H	H	OMe	COOH	H	2150	65
7	Cl	F	H	OMe	COOH	H	210	2
8	Cl	F	H	Cl	COOH	H	160	1.3
9	F	H	H	OMe	COOMe	H	15000	nd
10	Cl	Cl	H	H	H	OH	970	29
11	Cl	H	H	OMe	H	OH	65	8
12	Cl	Cl	H	H	COOH	H	7000	nd
13	Cl	Cl	H	H	COOH	OH	540	17
14	Cl	F	H	H	COOH	OH	510	8
15	Cl	Cl	H	Cl	COOH	OH	150	11
16	Cl	F	H	OCF_3	COOH	H	150	1.8
17	Cl	F	H	H	OH	OH	120	12
18	Cl	F	H	Cl	tetrazole	H	190	4
19	Cl	F	H	OMe	$CONH_2$	H	300	nd
20	Cl	F	H	OCF_3	tetrazole	H	80	3.7
21	Cl	F	H	OMe	H	OH	23	6.2
22	Cl	F	H	Cl	SO_2NH_2	H	1550	16
23							10000	nd
24							10000	nd
25							10000	nd
26	Cl	F	H	Cl	H	SO_2NH_2	2000	43
27	Cl	F	H	H	COOH	NH_2	700	51
28	Cl	Cl	H	OMe	H	NO_2	11,000	nd
29	Cl	Cl	H	OMe	H	NH_2	3000	nd
30	Cl	Cl	H	Cl	H	NHCONHMe	160	8
31	Cl	Cl	H	Cl	H	NHCOMe	200	7
32	Cl	Cl	H	OMe	H	NHCOMe	300	23
33	Cl	Cl	H	OMe	CONHMe	H	410	18
34	Cl	F	H	OMe	COOH	OH	160	2
35	Cl	F	F	OMe	COOH	OH	50	0.6
36	Cl	F	H	OMe	CH_2OH	H	800	2.9
37	Br	H	H	OMe	COOH	H	1200	22
38	Cl	F	F	Cl	COOH	OH	90	0.5
39	Cl	F	F	OCH_2CF_3	COOH	H	450	9.6
40	Cl	F	F	Cl	H	NHCOMe	60	0.5
41	Cl	F	F	OMe	H	NHCOMe	60	0.6
42	Cl	F	F	OMe	H	NHCONHMe	53	0.38
43	Cl	F	F	OMe	5-methyltriazole	H	250	1.6
44							35000	nd
45							3500	24

[a] Values represent the mean of three experiments performed in duplicate; nd, not determined. [b] Enzyme and hepatocyte potency variance was <25% for all compounds.

= 0.9) for the molecules in the training set (**1**−**25** in Table 2, Figure 3b). The significance of the model is also supported by the statistical cost analysis performed in Catalyst, indicating a predictive correlation probability of 75−90% (see Experimental Section for further details). Furthermore, the predictive power of the pharmacophore hypothesis has been valuable for calculation of the biological activity for several molecules of subsequent synthesis cycles (Figure 3b and text below).

The 1.9 Å X-ray structure of **21** bound to hlGP revealed the detailed molecular interactions of the inhibitor within the AMP site of the target enzyme (Figure 3c). As expected from the high sequence similarity within the AMP site of the rabmGP and hlGP, molecular interactions of the acyl urea scaffold are maintained for both enzyme−inhibitor complexes. The 2-chloro-4-fluoro-substituted benzoyl ring (X) tightly packs against Trp67, Arg193, Val40′, and Lys41′, with

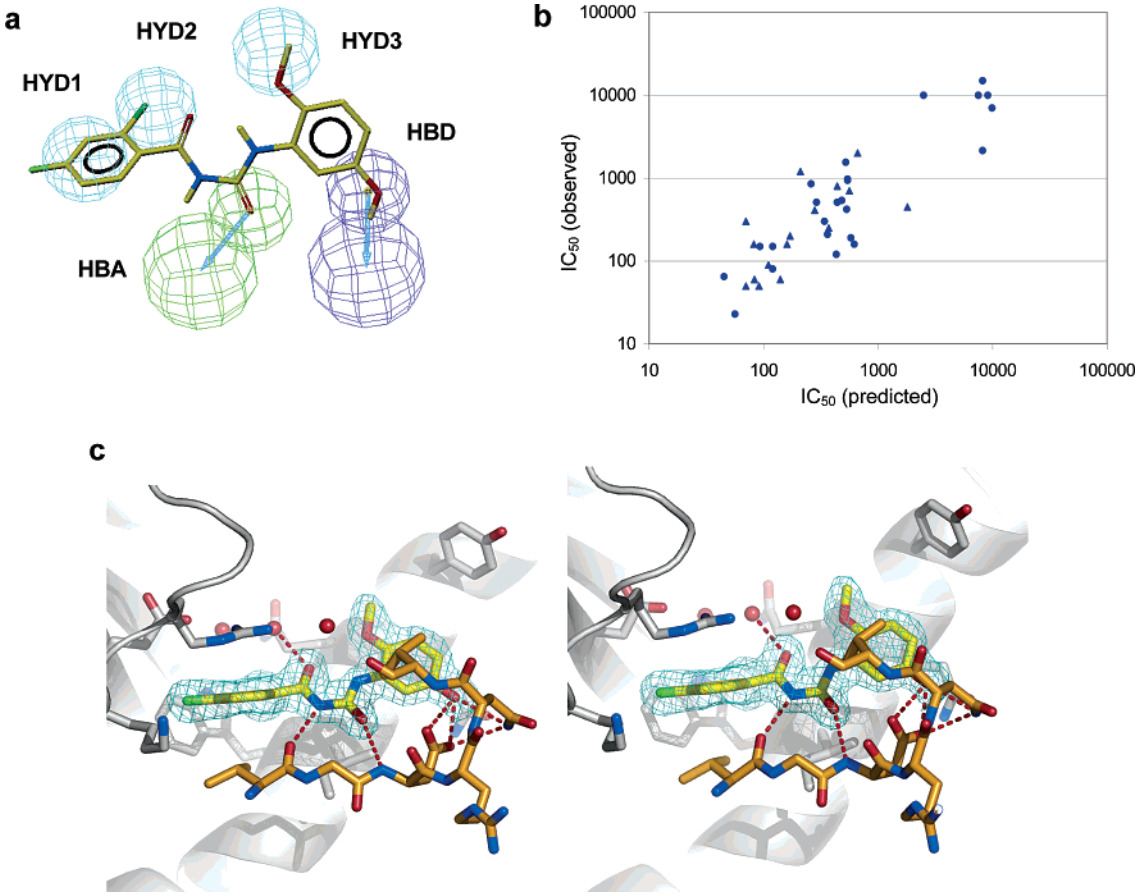

Figure 3. (a) Mapping of GP inhibitor **21** onto the Catalyst pharmacophore model. Pharmacophoric features are hydrogen-bond acceptors (HBA, green), hydrogen-bond donors (HBD, magenta), and hydrophobic groups (HYD, cyan). (b) Experimental vs calculated enzyme inhibitory activities (nM) of the training set (compounds **2**−**25**, ●) and "test set" (**26**, **27**, **30**−**43**, ▲) molecules based on 3D pharmacophore model. (c) Stereoview of the 1.9 Å structure of **21** bound to the AMP site of hlGPa. The AMP site resides at the dimer interface between monomer **1** (gray) and monomer **2** (Val40′, Lys41′ to Asn44′, Val45′; orange). The scaffold of the bound inhibitor (yellow) is well-defined in the $2F_o - F_c$ electron density (cyan; contour level at 1.0σ). The hydrogen-bonding network (red dashes) between the inhibitor and the main chain of Val40′ (2.7 Å), Asp42′ (3.4 Å), and an ordered water molecule in the upper part of the AMP pocket (2.7 Å) is maintained. Compared to the complex of **1** with rabmGPb, the phenol group of the inhibitor **21** forms additional hydrogen bonds with the carboxylate oxygens of Asp42′ (2.5 and 3.0 Å) and the NH_2 group of Asn44′ (3.1 Å). Steric clashes with Tyr75 as found for the screening hit **1** are eliminated. All distances correspond to subunit b.

the additional 4-fluoro substituent fitting nicely into the hydrophobic pocket formed by these side chains. In addition to these interactions, the modified substitution pattern of **21** provides additional recognition motifs mediating the improved enzyme inhibitory activity: (1) The phenolic ring (Y) reveals hydrophobic van der Waals interactions with Gln72. (2) Additional van der Waals interactions are mediated by the methoxy substituent positioned near Tyr75. (3) The phenolic ring (Y) induces additional hydrogen bonds between the side chains of Asp42′ and Asn44′ and the phenolic hydroxyl group. The experimentally determined conformation is in excellent agreement with the predicted conformation of compound **21** resulting from pharmacophore modeling.

Optimization of the Cellular Inhibitor Activity. Additional synthesis efforts aiming to improve the cellular activity of compound **21** were guided by information from the 3D pharmacophore and the 3D structure of the hlGPa inhibitor complex. Knowledge of the key chemical features required for the enzyme inhibitory activity supported the optimization of this series. Important chemical features were kept or replaced by corresponding bioisosteric groups within the subsequent synthesis steps, e.g. the phenolic hydroxyl group at Y5, a potential site of metabolism, was replaced by different hydrogen-bond-donor groups. In addition, variations in the benzoyl ring (X) were probed. The 3D pharmacophore hypothesis was used to predict the biological activity of the synthesis proposals in order to ensure that the synthesized molecules would retain good enzyme inhibitory activity while having improved cellular inhibitor activity. Molecules with a predicted biological activity in the micromolar range or below were chosen for synthesis. Table 2 shows the predicted values for biological activity for several compounds (**26**, **27**, **30**−**43**) that were subsequently synthesized. Mapping these molecules into Figure 3b reveals a good correlation between predicted and experimental enzyme inhibitory activities (correlation $R = 0.71$ for the "test set").[25]

Compounds **26**−**45** (see Scheme 2) were synthesized and tested for inhibitory activity in the hlGPa enzyme assay. Active compounds were tested in the rat hepatocyte assay (Table 1). Five out of the 20 derivatives revealed excellent inhibitory activity (IC_{50} below 100 nM) in the hlGPa enzyme assay. Of these, derivative **42** showed the best cellular activity. It inhibited the glycogen-derived glucose production by 50% at a concentration of 380 nM (hlGPa enzyme $IC_{50} = 53 \pm 1$ nM),

Table 2. Experimental Activities from the hlGPa Enzyme Assay and Predicted Activities in the Training Set Used for Pharmacophore Generation (**2**−**25**) and for the "Test Set" Used for Validation (**26**, **27**, **30**−**43**)

	IC_{50} (nM)		relative		IC_{50} (nM)		relative
compd	obsd	pred	error[a]	compd	obsd	pred	error[a]
2	940	540	−1.7	**22**	1550	520	−3.0
3	850	260	−3.3	**23**	10000	9100	−1.1
4	510	290	−1.8	**24**	10000	2500	−4.0
5	420	530	1.3	**25**	10000	7500	−1.3
6	2150	8200	3.8	**26**	2000	660	−3.0
7	210	360	1.7	**27**	700	560	−1.2
8	160	620	3.9	**30**	160	160	1
9	15000	8200	−1.8	**31**	200	170	−1.2
10	970	540	−1.8	**32**	300	70	−4.3
11	65	45	−1.4	**33**	410	280	−1.5
12	7000	9900	1.4	**34**	160	82	−2.0
13	540	480	−1.1	**35**	50	70	1.4
14	510	440	−1.1	**36**	800	440	−1.8
15	150	93	−1.6	**37**	1200	210	−5.7
16	150	120	−1.2	**38**	90	110	1.2
17	120	430	3.6	**39**	450	1800	3.9
18	190	580	3.1	**40**	60	140	2.3
19	300	340	1.1	**41**	60	83	1.4
20	80	120	1.6	**42**	53	91	1.8
21	23	56	2.4	**43**	250	370	1.5

[a] The relative error given in the table expresses the ratio of observed/predicted or predicted/observed. A positive value indicated that the observed activity is better than that predicted, and a negative value indicates that the observed activity is worse than that predicted.

corresponding to a 16-fold improvement of the cellular activity compared to the phenol derivative **21**.

In Vivo Activity of the hlGPa Inhibitor 42. The pharmacological effect of compound **42** on blood glucose levels was studied in anaesthetized Wistar rats during glucagon-induced glycogenolysis (Figure 4). The experiment lasted 6 h, and blood glucose levels were monitored every 15 min. After a basal period of 2 h, 1 mg of glucagon per rat was administered intravenously. In fed rats, glucagon produced a hyperglycemic response that lasted for 2 h. Intravenous administration of 5 mg/kg doses of **42** 15 min prior the glucagon injection caused a significant reduction of the glucagon-induced hyperglycemic peak. This observation is consistent with the inhibition of hepatic glycogen phosphorylase as the mode of action of **42**.[26]

3D QSAR Model for hlGPa Enzyme Inhibitor Activity. The chemical optimization was guided by the 3D pharmacophore model and by 3D structural information from the inhibitor−enzyme complexes. In addition, along the lead optimization process, several 3D QSAR models have been generated and used for a quantitative affinity prediction. Synthesis proposals were captured in virtual compound libraries and were prioritized on the basis of these constantly improving 3D QSAR models. The complete 3D QSAR has been captured in a final CoMFA model that has been generated on the basis of all benzoylphenyl ureas described in this study (Table 3). The descriptive and predictive abilities of the model are underscored by the statistic parameters $r^2 = 0.92$ and $q^2 = 0.66$. Figure 5a shows a plot of experimentally determined versus calculated pIC_{50}s.

The model is illustrated in Figures 5b−d, using contour maps along with the most active hlGPa inhibitor, **21** ($IC_{50} = 23 \pm 1$ nM), and two less active hlGPa inhibitors, **12** ($IC_{50} = 7$ μM) and **28** ($IC_{50} = 11$ μM). The

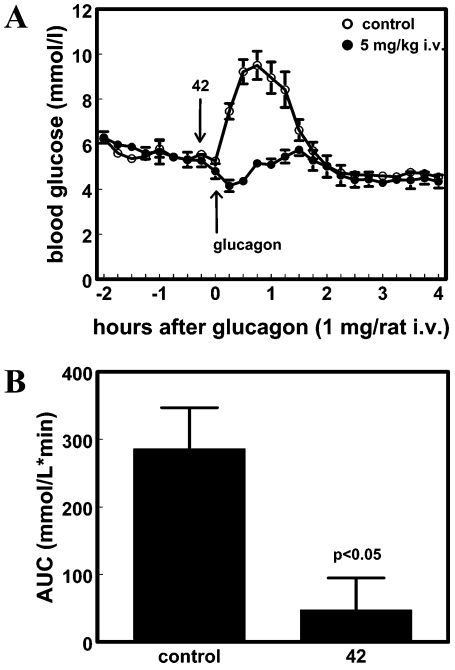

Figure 4. Effect of compound **42** on blood glucose in Wistar rats during glucagon-induced glycogenolysis at 5 mg/kg iv. (A) Blood glucose levels over time, values are mean ± SEM, n = 3−4. (B) AUC for glucose. AUC was calculated from time 0 (glucagon injection) until the end of the study and represents the area above the individual blood glucose values at time 0. Statistical differences were calculated by the Students t-test, and a value of $p < 0.05$ was considered as significant.

Table 3. Experimental Activity from the hlGPa Enzyme Assay and the Estimated Activity in the 3D QSAR Training Set

	IC_{50} (nM)	−log IC_{50}			IC_{50} (nM)	−log IC_{50}	
compd	obsd	obsd	pred	compd	obsd	obsd	pred
2	940	6.03	6.25	**26**	2000	5.69	5.53
3	850	6.07	6.20	**27**	700	6.15	6.08
4	510	6.29	6.06	**28**	11000	4.95	5.13
5	420	6.38	6.10	**29**	3000	5.53	6.04
6	2150	5.67	5.27	**30**	160	6.80	6.78
7	210	6.68	6.61	**31**	200	6.70	6.66
8	160	6.80	6.66	**32**	300	6.52	6.62
9	15000	4.82	4.99	**33**	410	6.39	6.07
10	970	6.01	6.00	**34**	160	6.80	7.20
11	65	7.19	6.89	**35**	50	7.30	7.16
12	7000	5.15	5.31	**36**	800	6.08	6.19
13	540	6.27	5.94	**37**	1200	5.92	6.15
14	510	6.29	6.49	**38**	90	7.05	7.19
15	150	6.82	6.69	**39**	450	6.35	6.31
16	150	6.82	6.95	**40**	60	7.22	7.16
17	120	6.92	7.03	**41**	60	7.22	7.13
18	190	6.72	6.93	**42**	53	7.28	7.24
19	300	6.52	6.60	**43**	250	6.60	6.52
20	80	7.10	7.27	**44**	35000	4.56	4.78
21	23	7.64	7.31	**45**	3500	5.46	5.26

model explains the high activity seen for compound **21** as well as the only moderate activity of compounds **12** and **28**, both of which fail to position appropriate chemical groups into regions that are positively correlated with biological activity.

As seen in Figure 5b, the ortho methoxy substituent of **21** is positioned within a region favoring steric bulk (green). The negatively charged hydroxyl oxygen atom at the 5-position of the phenyl ring (Y) is placed into a region where negative partial charge is correlated positively with the biological activity (red). The posi-

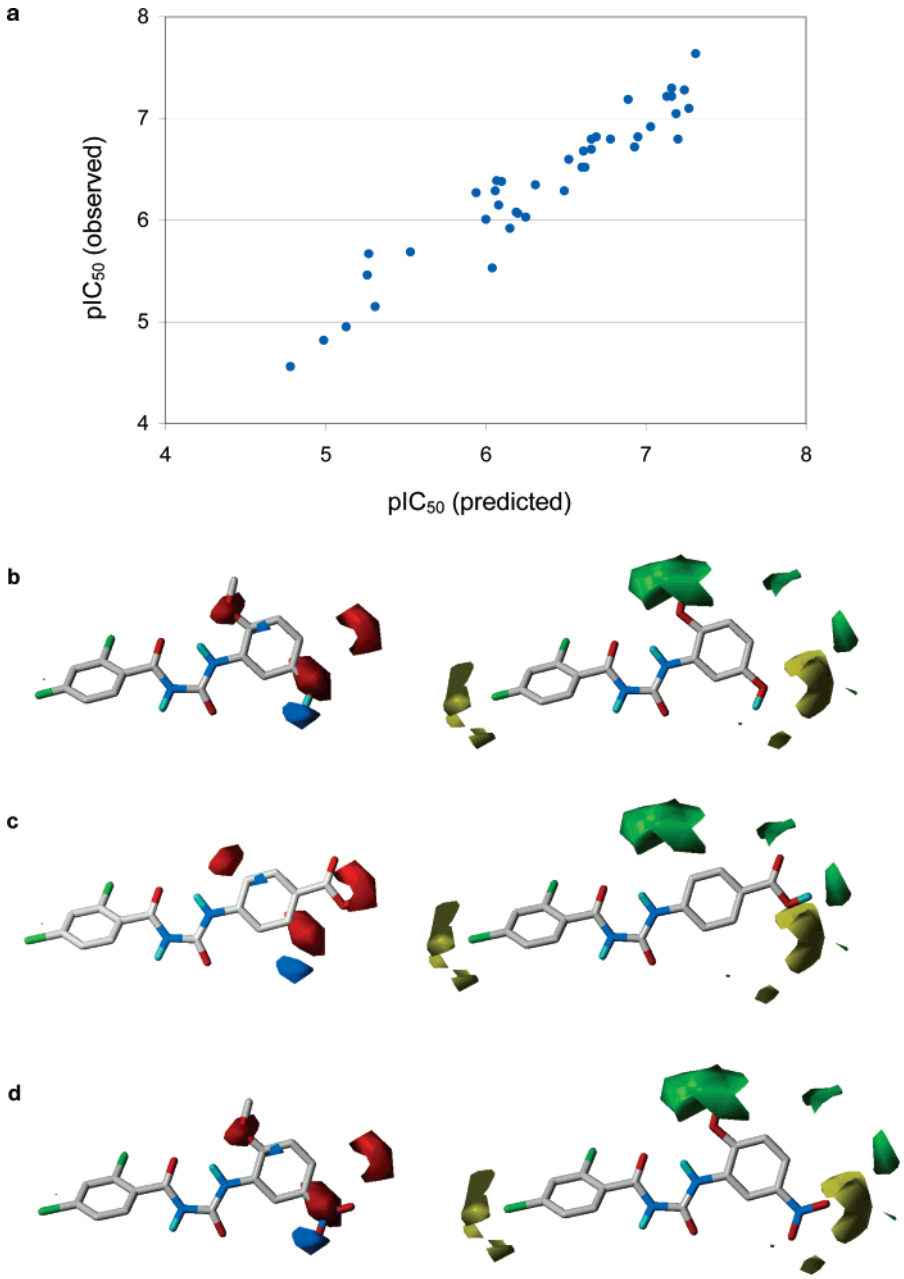

Figure 5. (a) Experimental vs calculated enzyme inhibitory activities (pIC_{50}) based on the 3D QSAR model. (b−d) View of the steric and electrostatic CoMFA STDV*COEFF contour maps. Regions where increasing steric bulk increases the potency of the hlGPa inhibitors are green and regions where increasing bulk decreases potency are yellow. The electrostatic contours indicate an increase of potency with increasing positive partial charge (blue) and negative charge (red), respectively. The most potent nanomolar hlGPa inhibitor **21** (b) and the less potent micromolar inhibitors **12** (c) and **28** (d) are shown along with the contour maps (left, electrostatic; right, steric).

tively charged hydroxyl hydrogen atom at the 5-position of the phenyl ring (Y) is located at a position where positive partial charge is beneficial (blue).

Figure 5c,d reveals the mapping of two less active compounds into the CoMFA contour maps. Although the benzoic acid derivative **12** places the negatively charged carboxylate substituent at the 4-position into a region where negative charge appears to be beneficial for the potency of this series, the compound lacks the steric bulk in the 2-position as well as the electrostatically favorable hydroxyl group in the 5-position, explaining the only moderate potency of 7 μM. Compound **28** places a sterically demanding methoxy group into the region where steric bulk is positively correlated with potency (Figure 5d, right). However, the nitro group in the 5-position of the aromatic ring positions the positively charged nitrogen atom in a region where negative charge is required for potency. The negatively charged oxygen atom of the nitro group falls into a region where negative charge is detrimental for the activity, explaining the low potency of this compound of 11 μM.

A comparison of the CoMFA model with the experimentally determined 3D structure is shown in Figure 6. The CoMFA contour maps have been superimposed onto the experimentally derived structure of the complex of the hlGPa inhibitor **21** and hlGPa. The superimposition reveals complementarities of the 3D QSAR model and the complex structure and illustrates the structural

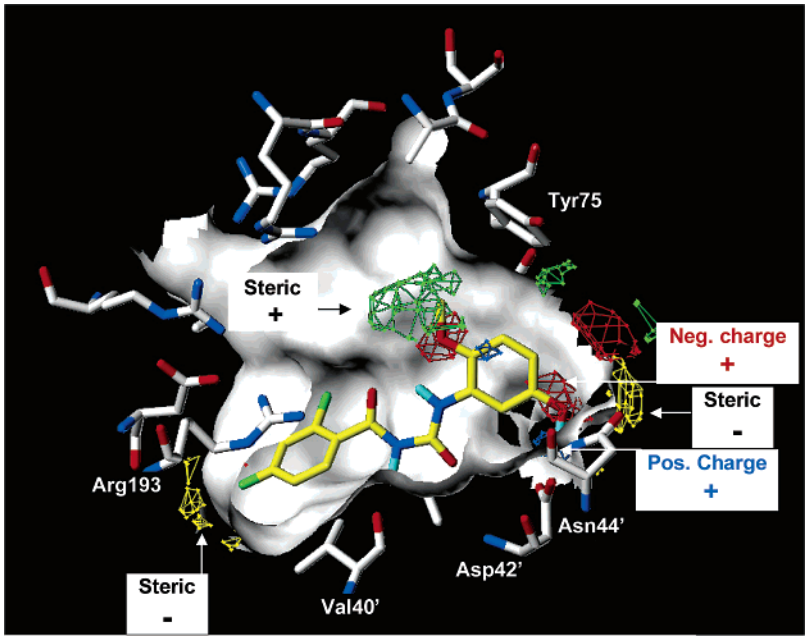

Figure 6. Steric and electrostatic CoMFA contour maps superimposed on the experimentally determined binding mode of the hlGPa inhibitior **21**. As in Figure 5, regions where increasing steric bulk increases the potency of the inhibitors are green, and regions where increasing bulk decreases activity are yellow. The electrostatic contours indicate an increase of activity with increasing positive partial charge (blue) and negative charge (red), respectively.

basis for the main steric and electrostatic interactions found within the CoMFA maps. The main contribution to the steric fields positively correlated with biological activity results from the methoxy substituent placed next to the Tyr75 (green region). Regions of steric hindrance (yellow) are found outside the solvent accessible surface of the binding site, indicating that derivatives having bulky substitutents in the 4-position of the benzoyl ring (X) or sterically demanding substituents in the 4- or 5-position of the phenyl ring (Y) cannot be accommodated within the binding pocket without conformational changes of the aligned amino acid side chains. The superimposition of the CoMFA model and the complex structure also reflects the structural basis for the main electrostatic interactions: the hydroxyl group of the phenyl ring (Y) is ideally placed within the electrostatic contour maps, allowing hydrogen bonding toward the side chains of Asp42′ and Asn44′.

Conclusions

This study reports acyl ureas as a novel class of hlGPa inhibitors. Parallel synthesis and rational drug design were used to optimize the screening hit in two chemical optimization cycles. The first cycle improved the moderate potency of the initial structure (**1**, hlGPa $IC_{50} = 2$ μM, cellular activity $IC_{50} = 80$ μM) to a compound with excellent potency in the enzymatic assay (**21**, hlGPa $IC_{50} = 23 \pm 1$ nM) but resulted only in moderate improvement of cellular activity ($IC_{50} = 6.2$ μM). A second optimization cycle was directed toward the improvement of cellular activity and resulted in a compound with good biological activity (**42**, hlGPa $IC_{50} = 53 \pm 1$ nM; cellular activity $IC_{50} = 380$ nM). This compound inhibits the glucagon-stimulated increase of blood glucose levels at a dose of 5 mg/kg in Wistar rats, thereby supporting the supposed mechanism of action of this inhibitor class, which is the inhibition of hepatic glycogenolysis.

Within this study pharmacophore and 3D QSAR models, which are highly predictive within the parameter space described by the analogues prepared, have been combined with structure-based design approaches, which provided guidance for the design of compounds not covered by the existing structure−activity knowledge. This combination has been the key factor for an efficient chemical optimization program.

Experimental Section

Chemical Synthesis. Commercial solvents and other reagents were used as received without further purification. Melting points of compounds, as precipitated solids, were measured on a Buchi B-545 melting point apparatus. Column chromatography was carried out on Merck silica gel 60 (230−400 mesh). Reversed-phase high-pressure chromatography was conducted on an Abimed Gilson instrument using a LiChrospher 100 RP-18e (5 μm) column from Merck. LC−MS analyses were performed on Agilent Series 1100 systems using a YMC J'sphere ODS H80 20 × 2.1 mm (4 μm) column and a Merck Purosphere 55 × 2 mm (5 μm) column. Varying ratios of acetonitrile and 0.05% trifluoroacetic acid in water were used as solvent systems. NMR spectra were recorded in DMSO-d_6 either on a Bruker DRX 400, Bruker ARX 500, or Varian Unity Plus 300 spectrometer. Chemical shifts are reported as δ values from an internal tetramethylsilane standard. Mass spectral data were either obtained on a VG Bio-Q triple Quadropole mass spectrometer using electro spray ionization (ES+ or ES−) or a VG ZAB 2-SEQ mass spectrometer using FAB ionization. Acurate mass measurements have been conducted with a Bruker Apex III FTICR mass spectrometer. Purity and characterization of compounds were established by a combination of LC−MS, high-resolution mass spectrometry (HRMS), and NMR analytical techniques. Using the following procedures it was possible to synthesize the compounds **2**−**8**, **12**, **16**−**20**, **22**−**26**, **28**, **33**, **36**, **38**−**39**, and **43**−**44** and the first step of the syntheses of compounds **10**, **13**−**14**, **27**, **30**, and **31** in parallel. Ten vials were heated in a parallel synthesis block with magnetic stirring. LC−MS analyses determined the completion of the reaction.

3-Chloro-4-[3-(2-chlorobenzoyl)ureido]benzoic Acid (2). To a suspension of 500 mg (3.21 mmol) of 2-chlorobenzamide

in 10 mL of 1,2-dichloroethane was added 571 μL (6.65 mmol) of oxalyl dichloride and the mixture heated to reflux for 16 h. The solvent was removed in vacuo, and 5 mL of toluene was added. Evaporation twice in vacuo removed the oxalyl dichloride. The residue was dissolved in 1 mL of acetonitrile, and a solution of 275 mg (1.61 mmol) of 4-amino-3-chlorobenzoic acid in 9 mL of acetonitrile was added and the mixture refluxed for 2 h. After cooling to room temperature, the precipitate was filtered and washed with acetonitrile to give 496 mg (77%) of **2**: mp 221−223 °C; ^{1}H NMR (400 MHz, DMSO-d_6) δ 7.41−7.62 (m, 4 H), 7.68 (d, J = 7.8 Hz, 1 H), 7.93−8.00 (m, 1 H), 8.47 (d, J = 8.3 Hz, 1 H), 11.30 (s br, 1 H), 11.65 (s br, 1 H), 13.20 (s br, 1 H).

4-[3-(2-Chlorobenzoyl)ureido]-3-methoxybenzoic Acid (3). To a suspension of 255 mg (1.64 mmol) of 2-chlorobenzamide in 12 mL of 1,2-dichloroethane was added 240 μL (2.79 mmol) of oxalyl dichloride and the mixture heated to reflux for 16 h. The solvent was removed in vacuo, and 5 mL of toluene was added. Evaporation twice in vacuo removed the oxalyl dichloride. A solution of 167 mg (1.0 mmol) of 4-amino-3-methoxybenzoic acid in 10 mL of acetonitrile was added to the residue and the mixture refluxed for 2 h. After cooling to room temperature, the precipitate was filtered and washed with acetonitrile to give 310 mg (89%) of **3**: mp 256−258 °C; ^{1}H NMR (400 MHz, DMSO-d_6) δ 3.97 (s, 3 H), 7.46 (td, J = 7.4 Hz, J = 1.5 Hz, 1 H), 7.52−7.66 (m, 5 H), 8.32 (d, J = 8.6 Hz, 1 H), 11.10 (s br, 1 H), 11.43 (s br, 1 H), 12.89 (s br, 1 H); MS (ES) *m/z* 349.1/351.1 (M + H)$^+$. Anal. Calcd ($C_{16}H_{13}ClN_2O_5$): C, 55.10; H, 3.76; N, 8.03. Found: C, 55.45; H, 3.85; N, 7.87.

4-[3-(2,4-Dichlorobenzoyl)ureido]-3-methoxybenzoic Acid (4). To a suspension of 380 mg (2.00 mmol) of 2,4-dichlorobenzamide in 12 mL of 1,2-dichloroethane 240 μL (2.79 mmol) was added oxalyl dichloride and the mixture heated to reflux for 16 h. The solvent was removed in vacuo and 5 mL of toluene was added. Evaporation twice in vacuo removed the oxalyl dichloride. A solution of 167 mg (1.0 mmol) of 4-amino-3-methoxybenzoic acid in 10 mL of acetonitrile was added to the residue and the mixture refluxed for 2 h. After cooling to room temperature, the precipitate was filtered and washed with acetonitrile to give 380 mg (99%) of **4**: mp 268−270 °C; ^{1}H NMR (400 MHz, DMSO-d_6) δ 3.95 (s, 3 H), 7.55−7.59 (m, 2 H), 7.61 (dd, J = 8.3 Hz, J = 1.5 Hz, 1 H), 7.69 (d, J = 8.3 Hz, 1 H), 7.79 (d, J = 1.9 Hz, 1 H), 8.31 (d, J = 8.3 Hz, 1 H), 11.03 (s br, 1 H), 11.50 (s br, 1 H), 12.87 (s br, 1 H); MS (ES) *m/z* 383.1/385.1 (M + H)$^+$.

3-Chloro-4-[3-(2,4-dichlorobenzoyl)ureido]benzoic Acid (5). A solution of 1.58 g (9.30 mmol) of 4-amino-3-chlorobenzoic acid in 50 mL of acetonitrile was added to 2.00 g (9.3 mmol) of 2,4-dichlorobenzoyl isocyanate (synthesis as described for **28**) and the mixture refluxed for 3 h. The solvent was evaporated in vacuo and the residue was purified by HPLC [acetonitrile/(H_2O + 0.1% trifluoroacetic acid) = 5/95 to 100/0, 15 min] to give 2.8 g (79%) of **5**: ^{1}H NMR (300 MHz, DMSO-d_6) δ 7.58 (dd, J = 7.9 Hz, J = 2.3 Hz, 1 H), 7.73 (d, J = 7.9 Hz, 1 H), 7.82 (d, J = 2.3 Hz, 1 H), 7.94 (dd, J = 7.9 Hz, J = 1.9 Hz, 1 H), 8.04 (d, J = 1.9 Hz, 1 H), 8.48 (d, J = 7.9 Hz, 1 H), 11.19 (s br, 1 H), 11.66 (s br, 1 H), 13.15 (s br, 1 H); HRMS calcd for $C_{15}H_9Cl_3N_2O_4Na$ 408.952 011, found 408.952 155 (M + Na), Dev = 0.35 ppm.

4-[3-(2-Fluorobenzoyl)ureido]-3-methoxybenzoic Acid (6). To a suspension of 500 mg (3.59 mmol) of 2-fluorobenzamide in 10 mL of 1,2-dichloroethane was added 430 μL (5.01 mmol) of oxalyl dichloride and the mixture heated to reflux for 14 h. The solvent was removed in vacuo and 5 mL of toluene was added. Evaporation twice in vacuo removed the oxalyl dichloride. The residue was dissolved in 10 mL of acetonitrile, 309 mg (1.85 mmol) of 4-amino-3-methoxybenzoic acid was added, and the mixture refluxed for 3 h. After cooling to room temperature, the precipitate was filtered and washed with acetonitrile to give 583 mg (98%) of **6**: ^{1}H NMR (300 MHz, DMSO-d_6) δ 3.98 (s, 3 H), 7.30−7.40 (m, 2 H), 7.57 (s, 1 H), 7.60−7.78 (m, 3 H), 8.33 (d, J = 8.3 Hz, 1 H), 11.18 (s br, 1 H), 11.29 (s br, 1 H), 12.84 (s br, 1 H); MS (ES) *m/z* 333.1 (M + H)$^+$; HRMS calcd for $C_{16}H_{13}FN_2O_5Na$ 355.070 070 8, found (M + Na) 355.070 134, Dev = 0.18 ppm. Anal. Calcd ($C_{16}H_{13}FN_2O_5$): C, 57.83; H, 3.94; N, 8.43. Found: C, 58.19; H, 4.01; N, 8.46.

4-[3-(2-Chloro-4-fluorobenzoyl)ureido]-3-methoxybenzoic Acid (7). To a suspension of 200 mg (1.15 mmol) of 2-chloro-4-fluorobenzamide in 10 mL of 1,2-dichloroethane was added 153 μL (1.78 mmol) of oxalyl dichloride and the mixture heated to reflux for 14 h. The solvent was removed in vacuo and 5 mL of toluene was added. Evaporation twice in vacuo removed the oxalyl dichloride. The residue was dissolved in 12.5 mL of acetonitrile, 96 mg (0.58 mmol) of 4-amino-3-methoxybenzoic acid was added, and the mixture refluxed for 3 h. After cooling to room temperature the precipitate was filtered and washed with acetonitrile to give 205 mg (97%) of **7**: ^{1}H NMR (300 MHz, DMSO-d_6) δ 3.96 (s, 3 H), 7.36 (td, J = 8.6 Hz, J = 2.7 Hz, 1 H), 7.56 (d, J = 1.7 Hz, 1 H), 7.58−7.65 (m, 2 H), 7.74 (dd, J = 8.6 Hz, J = 6.1 Hz, 1 H), 8.32 (d, J = 8.3 Hz, 1 H), 11.06 (s br, 1 H), 11.42 (s br, 1 H), 12.85 (s br, 1 H); MS (ES) *m/z* 367.1/369.1 (M + H)$^+$; HRMS calcd for $C_{16}H_{12}ClFN_2O_5$ Na 389.031 098 5, found 389.031 118 (M + Na), Dev = 0.05 ppm.

3-Chloro-4-[3-(2-chloro-4-fluorobenzoyl)ureido]benzoic Acid (8). To a suspension of 200 mg (1.15 mmol) of 2-chloro-4-fluorobenzamide in 10 mL of 1,2-dichloroethane was added 153 μL (1.78 mmol) oxalyl dichloride and the mixture heated to reflux for 14 h. The solvent was removed in vacuo and 5 mL of toluene was added. Evaporation twice in vacuo removed the oxalyl dichloride. The residue was dissolved in 12.5 mL of acetonitrile, 99 mg (0.58 mmol) of 3-chloro-4-aminobenzoic acid was added, and the mixture refluxed for 3 h. After cooling to room temperature, the precipitate was filtered and washed with acetonitrile to give 185 mg (87%) of **8**: ^{1}H NMR (300 MHz, DMSO-d_6) δ 7.38 (td, J = 7.8 Hz, J = 3.0 Hz, 1 H), 7.62 (dd, J = 8.9 Hz, J = 3.0 Hz 1 H), 7.77 (dd, J = 8.9 Hz, J = 7.0 Hz, 1 H), 7.95 (dd, J = 8.1 Hz, J = 2.2 Hz, 1 H), 8.03 (d, J = 2.2 Hz, 1 H), 8.47 (d, J = 8.2 Hz, 1 H), 11.23 (s, 1 H), 11.64 (s, 1 H), 13.17 (s br, 1 H); MS (ES) *m/z* 369.2/371.2 (M − H)$^-$; HRMS calcd for $C_{15}H_9Cl_2FN_2O_4Na$ 392.981 561 5, found 392.981 634 (M + Na), Dev = 0.19 ppm. Anal. Calcd ($C_{15}H_9Cl_2FN_2O_4$): C, 48.54; H, 2.44; N, 7.55. Found: C, 48.73; H, 2.48; N, 7.45.

4-[3-(2-Fluorobenzoyl)ureido]-3-methoxybenzoic Acid Methyl Ester (9). 4-[3-(2-Fluorobenzoyl)ureido]-3-methoxybenzoic acid (20.5 mg, 0.06 mmol) and 1 mL of thionyl chloride were heated to 85 °C for 5 h. The thionyl chloride was evaporated in vacuo and 2 mL of methanol was added. The methanol was evaporated in vacuo to give 16 mg (75%) of **9**: ^{1}H NMR (300 MHz, DMSO-d_6) δ 3.85 (s, 3 H), 3.98 (s, 3 H), 7.30−7.42 (m, 2 H), 7.57 (d, J = 1.9 Hz, 1 H), 7.60−7.76 (m, 3 H), 8.35 (d, J = 9.0 Hz, 1 H), 11.18 (s, 1 H), 11.28 (s, 1 H); MS (ES) *m/z* 347.0 (M + H)$^+$; HRMS calcd for $C_{17}H_{15}FN_2O_5Na$ 369.085 720 9, found 369.085 804 (M + Na), Dev = 0.23 ppm.

1-(2,4-Dichlorobenzoyl)-3-(3-hydroxyphenyl)urea (10). To a suspension of 696 mg (3.7 mmol) of 2,4-dichlorobenzamide in 4 mL of dichloromethane was added 651 μL (7.58 mmol) of oxalyl dichloride and the mixture heated to reflux for 22 h. The solvent was removed in vacuo and 5 mL of toluene was added. Evaporation twice in vacuo removed the oxalyl dichloride. The residue was dissolved in 4 mL of acetonitrile, a solution of 277 mg (1.8 mmol) of acetic acid 3-aminophenyl ester in 4 mL of acetonitrile was added, and the mixture refluxed for 3 h. The solvent was evaporated in vacuo and the residue was purified by HPLC [acetonitrile/(H_2O + 0.1% trifluoroacetic acid) = 5/95 to 100/0, 15 min] to give 297 mg (44%) of acetic acid 3-[3-(2,4-dichlorobenzoyl)ureido]phenyl ester. To a solution of sodium methanolate (500 mg of sodium in 20 mL of methanol) was added 100 mg (0.27 mmol) of acetic acid 3-[3-(2,4-dichlorobenzoyl)ureido]phenyl ester and the mixture stirred at room temperature. The precipitate was filtered and washed with methanol to give 89 mg (quant.) of **10**: mp 214−216 °C; ^{1}H NMR (400 MHz, DMSO-d_6) δ 6.51 (dd, J = 8.1 Hz, J = 2.2 Hz, 1 H), 6.86 (d, J = 8.1 Hz, 1 H), 7.08−7.15 (m, 2 H), 7.55 (dd, J = 8.3 Hz, J = 2.2 Hz, 1 H),

7.65 (d, J = 8.3 Hz, 1 H), 7.76 (d, J = 2 Hz, 1 H), 9.48 (s, 1 H), 10.23 (s br, 1 H), 11.17 (s br, 1 H).

1-(2-Chlorobenzoyl)-3-(5-hydroxy-2-methoxyphenyl)-urea (11). To a suspension of 224 mg (1.44 mmol) of 2-chlorobenzamide in 10 mL of 1,2-dichloroethane was added 185 μL (2.15 mmol) of oxalyl dichloride and the mixture heated to reflux for 17 h. The solvent was removed in vacuo and 5 mL of toluene was added. Evaporation in vacuo removed the oxalyl dichloride. The residue was dissolved in 5 mL of acetonitrile and added to a solution of 100 mg (0.72 mmol) of 3-amino-4-methoxyphenol and 146 μL (0.72 mmol) of bis(trimethylsilyl)-acetamide in 5 mL of acetonitrile and the reaction mixture was refluxed for 4.5 h. The solvent was evaporated and the residue was purified by liquid chromatography using silica gel and ethyl acetate/heptane = 1/8 to 1/1 as eluent to give 137 mg (60%) of **11**: ^{1}H NMR (300 MHz, DMSO-d_6) δ 3.79 (s, 3 H), 6.43 (dd, J = 8.6 Hz, J = 3.4 Hz, 1 H), 6.90 (d, J = 8.6 Hz, 1 H), 7.42−7.66 (m, 4 H), 7.78 (d, J = 3.4 Hz, 1 H), 9.02 (s, 1 H), 10.83 (s br, 1 H), 11.24 (s br, 1 H); HRMS calcd for $C_{15}H_{13}ClN_2O_4Na$ 343.045 605 7, found 343.045 729 (M + Na), Dev = 0.36 ppm.

4-[3-(2,4-Dichlorobenzoyl)ureido]benzoic Acid (12). To a suspension of 950 mg (5.00 mmol) of 2,4-dichlorobenzamide in 10 mL of 1,2-dichloro-ethane was added 600 μL (6.99 mmol) of oxalyl dichloride and the mixture heated to reflux for 14 h. The solvent was removed in vacuo and 5 mL of toluene was added. Evaporation twice in vacuo removed the oxalyl dichloride. One-fifth (1.00 mmol) of the isocyanate was dissolved in 5 mL of acetonitrile, 69 mg (0.5 mmol) of 4-aminobenzoic acid was added, and the mixture refluxed for 3 h. After cooling to room temperature, the precipitate was filtered and washed with acetonitrile to give 162 mg (92%) of **12**: ^{1}H NMR (300 MHz, DMSO-d_6) δ 7.57 (dd, J = 7.8 Hz, J = 2.6 Hz, 1 H), 7.63−7.72 (m, 3 H), 7.78 (d, J = 2.6 Hz, 1 H), 7.92 (d, J = 7.8 Hz, 2 H), 10.54 (s br, 1 H), 11.33 (s br, 1 H), 12.79 (s br, 1 H); MS (ES) m/z 351.1/353.1 $(M + H)^+$; HRMS calcd for $C_{15}H_{10}Cl_2N_2O_4Na$ 374.990 983 3, found 374.991 163 (M + Na), Dev = 0.48 ppm. Anal. Calcd ($C_{15}H_9Cl_2FN_2O_4$): C, 51.01; H, 2.85; N, 7.93. Found: C, 51.05; H, 2.88; N, 7.91.

4-[3-(2,4-Dichlorobenzoyl)ureido]-2-hydroxybenzoic Acid (13). To a suspension of 250 mg (1.3 mmol) of 2,4-dichlorobenzamide in 4 mL of dichloromethane was added 170 μL (1.98 mmol) of oxalyl dichloride and the mixture heated to reflux for 16 h. The solvent was removed in vacuo and 2 mL of toluene was added. Evaporation twice in vacuo removed the oxalyl dichloride. The residue was dissolved in 5 mL of acetonitrile and a solution of 130 mg (0.67 mmol) of 7-amino-2,2-dimethylbenzo[1,3]dioxin-4-one in 5 mL of acetonitrile was added and refluxed for 3 h. After cooling to room temperature, 3 mL of acetonitrile was added and the precipitate was filtered and washed with acetonitrile to give 1-(2,4-dichlorobenzoyl)-3-(2,2-dimethyl-4-oxo-4*H*-benzo[1,3]dioxin-7-yl)urea in quantitative yield. 1-(2,4-Dichlorobenzoyl)-3-(2,2-dimethyl-4-oxo-4*H*-benzo[1,3]dioxin-7-yl)urea (20 mg, 0.05 mmol) was dissolved in 5 mL of trifluoroacetic acid/water = 4/1 and heated to 50 °C for 16 h. After cooling to room temperature the precipitate was filtered and washed with acetonitrile to give 12 mg (67%) of **13**: mp 242−244 °C; ^{1}H NMR (300 MHz, DMSO-d_6) δ 7.04 (dd, J = 8.6 Hz, J = 2.2 Hz, 1 H), 7.35 (d, J = 2.2 Hz, 1 H), 7.55 (dd, J = 8.2 Hz, J = 2.2 Hz, 1 H), 7.68 (d, J = 8.6 Hz, 1 H), 7.75 (d, J = 8.2 Hz, 2 H), 7.77 (d, J = 2.2 Hz, 1 H), 10.46 (s br, 1 H), 11.30 (s br, 1 H), 11.40 (s br, 1 H), 13.80 (s br, 1 H); HRMS calcd for $C_{15}H_{10}Cl_2N_2O_5Na$ 390.985 898, found 390.986 129 (M + Na), Dev = 0.59 ppm.

4-[3-(2-Chloro-4-fluorobenzoyl)ureido]-2-hydroxybenzoic Acid (14). To a suspension of 250 mg (1.4 mmol) of 2-chloro-4-fluorobenzamide in 4 mL of dichloromethane was added 190 μL (2.21 mmol) of oxalyl dichloride and the mixture heated to reflux for 16 h. The solvent was removed in vacuo and 2 mL of toluene was added. Evaporation twice in vacuo removed the oxalyl dichloride. The residue was dissolved in 5 mL of acetonitrile and a solution of 140 mg (0.72 mmol) of 7-amino-2,2-dimethylbenzo[1,3]dioxin-4-one in 5 mL of acetonitrile was added and the mixture refluxed for 3 h. After cooling to room temperature, 3 mL of acetonitrile was added and the precipitate was filtered and washed with acetonitrile to give 197 mg (70%) of 1-(2-chloro-4-fluorobenzoyl)-3-(2,2-dimethyl-4-oxo-4*H*-benzo[1,3]dioxin-7-yl)-urea. 1-(2-Chloro-4-fluorobenzoyl)-3-(2,2-dimethyl-4-oxo-4*H*-benzo[1,3]dioxin-7-yl)urea (20 mg, 0.05 mmol) was dissolved in 5 mL of trifluoroacetic acid/water = 4/1 and heated to 50 °C for 16 h. After cooling to room temperature, the precipitate was filtered and washed with acetonitrile to give 13 mg (73%) of **14**: ^{1}H NMR (300 MHz, DMSO-d_6) δ 7.05 (dd, J = 8.6 Hz, J = 2.3 Hz, 1 H), 7.31−7.42 (m, 2 H), 7.60 (dd, J = 8.6 Hz, J = 2.3 Hz, 1 H), 7.68−7.80 (m, 2 H), 10.52 (s br, 1 H), 11.30 (s br, 1 H), 11.4 (s br, 1 H), 13.8 (s br, 1 H).

5-Chloro-4-[3-(2,4-dichlorobenzoyl)ureido]-2-hydroxybenzoic Acid (15). To a suspension of 152 mg (0.80 mmol) of 2,4-dichlorobenzamide in 10 mL of 1,2-dichloroethane was added 104 μL (1.21 mmol) of oxalyl dichloride and the mixture heated to reflux for 15 h. The solvent was removed in vacuo and 5 mL of toluene was added. Evaporation in vacuo removed the oxalyl dichloride. The residue was dissolved in 5 mL of acetonitrile and added to a solution of 75 mg (0.40 mmol) of 4-amino-5-chloro-2-hydroxybenzoic acid and 99 μL (0.40 mmol) of bis(trimethylsilyl)acetamide in 5 mL of acetonitrile, and the reaction mixture was refluxed for 3 h. Addition of 2 mL of methanol caused the beginning of the precipitation. The reaction mixture was heated to 75 °C for 30 min. After cooling to room temperature, the reaction mixture was filtered and washed with acetonitrile to give 145 mg (90%) of **15**: ^{1}H NMR (300 MHz, DMSO-d_6) δ 7.60 (dd, J = 7.9 Hz, J = 2.3 Hz, 1 H), 7.72 (d, J = 7.9 Hz, 1 H), 7.79 (d, J = 2.3 Hz, 1 H), 7.83 (s, 1 H), 8.00 (s, 1 H), 11.20 (s br, 1 H), 11.68 (s br, 1 H); HRMS calcd for $C_{15}H_8Cl_3N_2O_5Na_2$ 446.928 870 3, found 446.929 193 (M − H + 2Na), Dev = 0.72 ppm. Anal. Calcd ($C_{15}H_9Cl_3N_2O_5$): C, 44.64; H, 2.24; N, 6.94. Found: C, 44.76; H, 2.34; N, 6.91.

4-[3-(2-Chloro-4-fluorobenzoyl)ureido]-3-trifluoromethoxybenzoic Acid (16). To a suspension of 174 mg (1.00 mmol) of 2-chloro-4-fluorobenzamide in 10 mL of 1,2-dichloroethane was added 120 μL (1.40 mmol) of oxalyl dichloride and the mixture heated to reflux for 14 h. The solvent was removed in vacuo and 5 mL of toluene was added. Evaporation twice in vacuo removed the oxalyl dichloride. The residue was dissolved in 10 mL of acetonitrile, 110 mg (0.5 mmol) of 4-amino-3-trifluoromethoxybenzoic acid was added, and the mixture refluxed for 3 h. After cooling to room temperature, the precipitate was filtered and washed with acetonitrile to give 160 mg (76%) of **16**: mp 245−246 °C; ^{1}H NMR (300 MHz, DMSO-d_6) δ 7.37 (td, J = 8.6 Hz, J = 2.5 Hz, 1 H), 7.63 (dd, J = 8.9 Hz, J = 2.5 Hz, 1 H), 7.77 (dd, J = 8.6 Hz, J = 6 Hz, 1 H), 7.90 (s, 1 H), 8.02 (dd, J = 10.4 Hz, J = 1.8 Hz, 1 H), 8.48 (d, J = 8.6 Hz, 1 H), 11.26 (s br, 1 H), 11.67 (s br, 1 H), 13.28 (s br, 1 H); MS (ES) m/z 418.9/420.9 $(M - H)^-$; HRMS calcd for $C_{16}H_9ClF_4N_2O_5Na$ 443.002 833, found 443.003 04 (M + Na), Dev = 0.47 ppm. Anal. Calcd ($C_{16}H_9ClF_4N_2O_5$): C, 45.68; H, 2.15; N, 6.66. Found: C, 45.86; H, 2.20; N, 6.93.

1-(2-Chloro-4-fluorobenzoyl)-3-(3,4-dihydroxyphenyl)-urea (17). To a suspension of 223 mg (1.28 mmol) of 2-chloro-4-fluorobenzamide in 10 mL of 1,2-dichloroethane was added 160 μL (1.86 mmol) of oxalyl dichloride and the mixture heated to reflux for 18 h. The solvent was removed in vacuo and 5 mL of toluene was added. Evaporation twice in vacuo removed the oxalyl dichloride. The residue was dissolved in 6 mL of acetonitrile, a solution of 65 mg (0.64 mmol) of 4-aminobenzene-1,2-diol and 314 μL (1.28 mmol) of bis(trimethylsilyl)-acetamide in 6 mL of acetonitrile was added, and the mixture refluxed for 3 h. After cooling to room temperature, the solvent was evaporated and the residue was purified by HPLC [acetonitrile/(H_2O + 0.1% trifluoroacetic acid) = 5/95 to 100/0, 15 min] to give 94 mg (45%) of **17**: ^{1}H NMR (300 MHz, DMSO-d_6) δ 6.64−6.73 (m, 2 H), 7.10 (d, J = 2.2 Hz, 1 H), 7.35 (td, J = 8.2 Hz, J = 2.6 Hz, 1 H), 7.58 (dd, J = 8.6 Hz, J = 2.6 Hz, 1 H), 7.70 (dd, J = 8.2 Hz, J = 6.7 Hz, 1 H), 8.72 (s, 1 H), 9.04 (s, 1 H), 10.10 (s br, 1 H), 11.07 (s br, 1 H); MS (ES) m/z 325.1/327.1 $(M + H)^+$; HRMS calcd for $C_{14}H_{10}ClFN_2O_4Na$ 347.020 533 8, found 347.020 59 (M + Na), Dev = 0.16 ppm.

Anal. Calcd ($C_{14}H_{10}ClFN_2O_4$): C, 51.79; H, 3.10; N, 8.63. Found: C, 52.11; H, 3.42; N, 8.67.

1-(2-Chloro-4-fluorobenzoyl)-3-[2-chloro-4-(1*H*-tetrazol-5-yl)phenyl]urea (18). To a suspension of 1.04 g (6.0 mmol) of 2-chloro-4-fluorobenzamide in 3 mL of dichloromethane was added 800 μL (9.32 mmol) of oxalyl dichloride and the mixture heated to reflux for 9 h. The solvent was removed in vacuo and 2 mL of toluene was added. Evaporation twice in vacuo removed the oxalyl dichloride to give 1.17 g (97%) of 2-chloro-4-fluorobenzoyl isocyanate. A solution of 110 mg (0.55 mmol) of the isocyanate in 0.5 mL of dichloromethane was added to a suspension of 100 mg (0.5 mmol) of 2-chloro-4-(1*H*-tetrazol-5-yl)phenylamine in 3 mL of acetonitrile and the mixture heated to 40 °C for 2 h. After cooling to room temperature, the precipitate was filtered, washed with acetonitrile, and dried in vacuo to give 150 mg (76%) **18**: mp 227−228 °C; ^{1}H NMR (400 MHz, DMSO-d_6) δ 7.38 (td, J = 8.6 Hz, J = 2.4 Hz, 1 H), 7.62 (dd, J = 9.0 Hz, J = 2.4 Hz, 1 H), 7.77 (dd, J = 8.6 Hz, J = 6.1 Hz, 1 H), 8.06 (dd, J = 8.8 Hz, J = 2.2 Hz, 1 H), 8.20 (d, J = 2.0 Hz, 1 H), 8.54 (d, J = 8.8 Hz, 1 H), 11.22 (s br, 1 H), 11.63 (s br, 1 H).

4-[3-(2-Chloro-4-fluorobenzoyl)ureido]-3-methoxybenzamide (19). To a suspension of 104 mg (0.60 mmol) of 2-chloro-4-fluorobenzamide in 4 mL of 1,2 dichloroethane was added 80 μL (0.93 mmol) of oxalyl dichloride and the mixture heated to reflux for 16 h. The solvent was removed in vacuo and 2 mL of toluene was added. Evaporation twice in vacuo removed the oxalyl dichloride. The residue was dissolved in 5 mL of acetonitrile, a solution of 100 mg (0.60 mmol) of 4-amino-3-methoxybenzamide in 5 mL of acetonitrile was added, and the mixture refluxed for 4 h. After cooling to room temperature, 3 mL of acetonitrile was added, and the precipitate was filtered and washed with acetonitrile to give 167 mg (77%) of **19**: mp 268−270 °C; ^{1}H NMR (300 MHz, DMSO-d_6) δ 3.98 (s, 3 H), 7.13 (s, 1 H), 7.24−7.65 (m, 4 H), 7.76 (dd, J = 8.2 Hz, J = 5.9 Hz, 1 H), 7.98 (s br, 1 H), 8.26 (d, J = 8.2 Hz, 1 H), 10.98 (s br, 1 H), 11.39 (s br, 1 H); HRMS calcd for $C_{16}H_{13}ClFN_3O_4$ 366.065 138 3, found 366.065 237 (M + H), Dev = 0.27 ppm.

1-(2-Chloro-4-fluorobenzoyl)-3-[4-(1*H*-tetrazol-5-yl)-2-trifluoromethoxyphenyl]urea (20). To a suspension of 100 mg (0.4 mmol) of 4-(1*H*-tetrazol-5-yl)-2-trifluoromethoxyphenylamine in 1.5 mL of acetonitrile was added a solution of 90 mg (0.45 mmol) 2-chloro-4-fluorobenzoyl isocyanate (synthesis as described for **18**) in 0.4 mL of dichloromethane and the mixture stirred at room temperature for 2 h. The precipitate was filtered, washed with acetonitrile, and dried in vacuo to give 56 mg (31%) of **20**: mp 275−277 °C; ^{1}H NMR (400 MHz, DMSO-d_6) δ 7.37 (td, J = 8.6 Hz, J = 2.5 Hz, 1 H), 7.62 (dd, J = 9.0 Hz, J = 2.5 Hz, 1H), 7.77 (dd, J = 8.6 Hz, J = 6.1 Hz, 1 H), 8.08−8.15 (m, 2 H), 8.56 (d, J = 8.6 Hz, 1 H), 11.23 (s, 1 H), 11.65 (s, 1 H).

1-(2-Chloro-4-fluorobenzoyl)-3-(5-hydroxy-2-methoxyphenyl)urea (21). To a suspension of 124 mg (0.72 mmol) of 2-chloro-4-fluorobenzamide in 5 mL of 1,2-dichloroethane was added 92 μL (1.07 mmol) of oxalyl dichloride and the mixture heated to reflux for 17 h. The solvent was removed in vacuo and 3 mL of toluene was added. Evaporation in vacuo removed the oxalyl dichloride. The residue was dissolved in 2.5 mL of acetonitrile and added to a solution of 50 mg (0.36 mmol) of 3-amino-4-methoxyphenol and 73 μL (0.36 mmol) bis(trimethylsilyl)acetamide in 2.5 mL of acetonitrile, and the reaction mixture was refluxed for 4 h. The solvent was evaporated and the residue was purified by liquid chromatography using silica gel and ethyl acetate/heptane = 1/1 as eluent followed by HPLC [acetonitrile/(H_2O + 0.1% trifluoroacetic acid) = 5/95 to 100/0, 15 min] to give 23 mg (19%) of **21**: ^{1}H NMR (300 MHz, DMSO-d_6) δ 3.79 (s, 3 H), 6.42 (dd, J = 7.9 Hz, J = 3.4 Hz, 1 H), 6.88 (d, J = 9.4 Hz, 1 H), 7.36 (td, J = 9.7 Hz, J = 3.4 Hz, 1 H), 7.59 (dd, J = 9.4 Hz, J = 3.4 Hz, 1 H), 7.68−7.77 (m, 2 H), 9.02 (s, 1 H), 10.78 (s br, 1 H), 11.26 (s br, 1 H); HRMS calcd for $C_{15}H_{12}ClFN_2O_4Na$ 361.036 183 9, found 361.036 298 (M + Na), Dev = 0.32 ppm.

3-Chloro-4-[3-(2-chloro-4-fluorobenzoyl)ureido]benzenesulfonamide (22). To a suspension of 100 mg (0.4 mmol) of 4-amino-3-chlorobenzenesulfonamide in 1.5 mL of acetonitrile was added a solution of 110 mg (0.55 mmol) of 2-chloro-4-fluorobenzoyl isocyanate (synthesis as described for **18**) in 0.5 mL of dichloromethane and the mixture stirred at room temperature for 10 min. The precipitate was filtered, washed with acetonitrile, and dried in vacuo to give 150 mg (74%) of **22**: ^{1}H NMR (400 MHz, DMSO-d_6) δ 7.37 (td, J = 8.6 Hz, J = 2.4 Hz, 1 H), 7.45 (s, 2 H), 7.62 (dd, J = 9.0 Hz, J = 2.4 Hz, 1 H), 7.77 (dd, J = 8.6 Hz, J = 6.1 Hz, 1 H), 7.81 (dd, J = 8.8 Hz, J = 2.1 Hz, 1 H), 7.95 (d, J = 2.1 Hz, 1 H), 8.50 (d, J = 8.8 Hz, 1 H), 11.22 (s br, 1 H), 11.64 (s br, 1 H).

1-(2-Chloro-4-fluorobenzoyl)-3-(4-methylthiazol-2-yl)-urea (23). To a suspension of 160 mg (1.4 mmol) of 4-methylthiazol-2-ylamine in 2 mL of acetonitrile was added a solution of 280 mg (1.4 mmol) of 2-chloro-4-fluorobenzoyl isocyanate (synthesis as described for **18**) in 1.3 mL dichloromethane at 0 °C and the mixture stirred at room temperature for 1 h. The precipitate was filtered, washed with acetonitrile, and dried in vacuo to give 255 mg (58%) of **23**: ^{1}H NMR (300 MHz, DMSO-d_6) δ 2.28 (s, 3 H), 6.84 (s, 1 H), 6.86 (s, 1 H), 7.38 (td, J = 7.5 Hz, J = 2.8 Hz, 1 H), 7.62 (dd, J = 9.4 Hz, J = 2.8 Hz, 1 H), 7.78 (dd, J = 9.4 Hz, J = 7.5 Hz, 1 H), 11.55 (s br, 1 H).

3-(4-Chlorophenylsufonyl)-1-[4-(1*H*-tetrazol-5-yl)-2-trifluoromethoxyphenyl]urea (24). To a solution of 100 mg (0.4 mmol) of 4-(1*H*-tetrazol-5-yl)-2-trifluoromethoxyphenylamine in 1.5 mL of acetonitrile was added 98 mg (0.45 mmol) of 4-chlorobenzenesulfonyl isocyanate and the mixture stirred at room temperature for 2 h. The precipitate was filtered, washed with acetonitrile, and dried in vacuo to give 80 mg (43%) of **24**: ^{1}H NMR (400 MHz, DMSO-d_6) δ 7.45 (s br, 1 H), 7.74 (m, 2 H), 8.02 (m, 4 H), 8.28 (m, 1 H), 8.81 (s, 1 H).

4-[3-(2-Chloro-4-fluorobenzoyl)ureidomethyl]benzoic Acid (25). To a suspension of 107 mg (0.7 mmol) of 4-aminobenzoic acid in 3 mL of acetonitrile was added a solution of 77 mg (0.77 mmol) of 2-chloro-4-fluorobenzoyl isocyanate (synthesis as described for **18**) in 0.7 mL dichloromethane and the mixture stirred at room temperature for 10 min. The precipitate was filtered, washed with acetonitrile, and dried in vacuo to give 130 mg (53%) of **25**: ^{1}H NMR (400 MHz, DMSO-d_6) δ 4.49 (d, J = 6.1 Hz, 2 H), 7.30 (m, 1 H), 7.39−7.50 (m, 3 H), 7.55 (m, 1 H), 7.66 (m, 1 H), 7.90 (m, 3 H), 8.84 (m, 1 H).

4-Chloro-3-[3-(2-chloro-4-fluorobenzoyl)ureido]benzenesulfonamide (26). To a suspension of 270 mg (1.3 mmol) of 3-amino-4-chlorobenzenesulfonamide in 5 mL of acetonitrile was added a solution of 280 mg (1.4 mmol) of 2-chloro-4-fluorobenzoyl isocyanate (synthesis as described for **18**) in 1.3 mL of dichloromethane and the mixture heated to 50 °C for 2 h. After cooling to room temperature the precipitate was filtered, washed with acetonitrile, and dried in vacuo to give 400 mg (76%) of **26**: mp 209−211 °C; ^{1}H NMR (400 MHz, DMSO-d_6) δ 7.38 (td, J = 7.7 Hz, J = 2.6 Hz, 1 H), 7.50 (s br, 2 H), 7.59 (d, J = 9.7 Hz, 1 H), 7.61 (d, J = 9.7 Hz, 1 H), 7.78 (m, 2 H), 8.83 (s, 1 H), 11.20 (s, 1 H), 11.70 (s, 1 H).

2-Amino-4-[3-(2-chloro-4-fluorobenzoyl)ureido]benzoic Acid (27). To a suspension of 206 mg (1.19 mmol) of 2-chloro-4-fluorobenzamide in 10 mL of 1,2-dichloroethane was added 155 μL (1.80 mmol) of oxalyl dichloride and the mixture heated to reflux for 17 h. The solvent was removed in vacuo and 5 mL of toluene was added. Evaporation in vacuo removed the oxalyl dichloride. The residue was dissolved in 5 mL of acetonitrile and a solution of 150 mg (0.59 mmol) of 4-amino-2-*tert*-butoxycarbonylaminobenzoic acid in 5 mL of acetonitrile was added. After 5 min, the precipitate was filtered and washed with acetonitrile to give 124 mg (46%) of 2-*tert*-butoxycarbonylamino-4-[3-(2-chloro-4-fluorobenzoyl)ureido]-benzoic acid. This product was suspended in 0.5 mL of DMF and 3 mL of trifluoroacetic acid and the mixture stirred for 4 h. The precipitate was filtered and washed with methanol, and the filtrate was evaporated in vacuo. To the residue was added 5 mL of water, and the precipitate was filtered and washed with water. The precipitate was purified by HPLC [acetonitrile/(H_2O + 0.1% trifluoroacetic acid) = 5/95 to 100/0, 15 min]

to give 15 mg (35%) of **27**: mp 221−223 °C; ^{1}H NMR (400 MHz, DMSO-d_6) δ 6.60 (dd, J = 7.9 Hz, J = 1.9 Hz, 1 H), 7.13 (d, J = 1.9 Hz, 1 H), 7.38 (td, J = 8.2 Hz, J = 3.4 Hz, 1 H), 7.57−7.78 (m, 3 H), 10.37 (s br, 1 H), 11.23 (s br, 1 H); HRMS calcd for $C_{15}H_{11}ClFN_3O_4Na$ 374.031 432 9, found 374.031 712 (M + Na), Dev = 0.75 ppm.

1-(2,4-Dichlorobenzoyl)-3-(2-methoxy-5-nitrophenyl)-urea (28). To a suspension of 100 g (0.53 mol) of 2,4-dichlorobenzamide in 300 mL of dichloromethane was added 133.6 g (1.05 mol) of oxalyl dichloride at 5 °C and the mixture heated to reflux for 14 h. The solvent was removed in vacuo and 50 mL of toluene was added. Evaporation three times in vacuo removed the oxalyl dichloride to give 110 g of 2,4-dichlorobenzoyl isocyanate. The isocyanate (1.29 g, 5.90 mmol) was added to a solution of 1.00 g (5.9 mmol) of 2-methoxy-5-nitro-phenylamine in 10 mL of acetonitrile and the mixture heated to 50 °C for 2 h. After cooling to room temperature, the precipitate was filtered and washed with acetonitrile to give 2.00 g (88%) of **28**: ^{1}H NMR (500 MHz, DMSO-d_6) δ 4.11 (s, 3H), 7.33 (d, J = 9.3 Hz, 1H), 7.58 (dd, J = 8.3 Hz, J = 2.0 Hz, 1H), 7.70 (d, J = 8.3 Hz, 1 H), 7.80 (d, J = 2.0 Hz, 1 H), 8.07 (dd, J = 9.3 Hz, J = 2.9 Hz, 1 H), 9.11 (d, J = 2.9 Hz, 1 H), 11.05 (s br, 1 H), 11.60 (s br, 1 H); HRMS calcd for $C_{15}H_{11}Cl_2N_3O_5Na$ 405.996 797, found 405.997 12 (M + Na), Dev = 0.80 ppm. Anal. Calcd ($C_{15}H_{11}Cl_2N_3O_5$): C, 46.89; H, 2.89; N, 10.94. Found: C, 47.18; H, 3.09; N, 10.98.

1-(5-Amino-2-methoxyphenyl)-3-(2,4-dichlorobenzoyl)-urea (29). 28 (2.00 g, 5.2 mmol) was suspended in 50 mL of ethyl acetate and the mixture heated to reflux. $SnCl_2{\cdot}H_2O$ (5.86 g, 26.0 mmol) was added and the reaction mixture was refluxed for 1 h. After cooling to room temperature, the precipitate was filtered and washed with ethyl acetate to give 1.60 g (87%) of **29**: ^{1}H NMR (500 MHz, DMSO-d_6) δ 3.93 (s, 3 H), 7.03 (dd, J = 8.6 Hz, J = 2.2 Hz, 1 H), 7.18 (d, J = 8.6 Hz, 1H), 7.57 (d, J = 7.4 Hz, 1 H), 7.68 (d, J = 7.4 Hz, 1 H), 7.78 (s, 1 H), 8.26 (d, J = 2.2 Hz, 1 H), 9.70 (s br, 3 H), 10.95 (s br, 1 H), 11.44 (s, 1 H); HRMS calcd for $C_{15}H_{13}Cl_2N_3O_3$ 354.040 673 2, found 354.040 892 (M + H), Dev = 0.62 ppm.

1-{4-Chloro-3-[3-(2,4-dichlorobenzoyl)ureido]phenyl}-3-methylurea (30). 2,4-Dichloro-benzoyl isocyanate (1.25 g, 5.80 mmol) (synthesis as described for **28**) was added to a solution of 1.00 g (5.8 mmol) of 2-chloro-5-nitro-phenylamine in 10 mL of acetonitrile and the mixture heated to 50 °C for 2 h. After cooling to room temperature, the precipitate was filtered and washed with acetonitrile to give 2.00 g (89%) of 1-(2-chloro-5-nitrophenyl)-3-(2,4-dichlorobenzoyl)urea. 1-(2-Chloro-5-nitrophenyl)-3-(2,4-dichlorobenzoyl)urea (2.00 g, 5.2 mmol) was suspended in 30 mL of ethyl acetate and the mixture heated to reflux. $SnCl_2{\cdot}H_2O$ (4.90 g, 21.7 mmol) was added and the mixture refluxed for 1 h. After cooling to room temperature, the precipitate was filtered and washed with ethyl acetate to give 1.60 g (87%) of 1-(5-amino-2-chlorophenyl)-3-(2,4-dichlorobenzoyl)urea. 1-(5-Amino-2-chlorophenyl)-3-(2,4-dichlorobenzoyl)urea (100 mg, 0.28 mmol) was dissolved in 5 mL of *N*-methylpyrrolidone, which was warmed to 50 °C, 16 mg (0.28 mmol) of isocyanatomethane was added, and the mixture heated to 50 °C for 15 min. After cooling to room temperature, the precipitate was filtered and washed with acetonitrile. The residue was purified by HPLC [acetonitrile/(H_2O + 0.1% trifluoroacetic acid) = 5/ 95 to 100/0, 15 min] to give 5 mg (4%) of **30**: ^{1}H NMR (500 MHz, DMSO-d_6) δ 2.65 (d, J = 4.6 Hz, 3 H), 5.99 (q, J = 4.6 Hz, 1 H), 7.37 (d, J = 8.6 Hz, 1H), 7.43 (d, J = 8.6 Hz, 1 H), 7.56 (d, J = 8.0 Hz, 1 H), 7.70 (d, J = 8.0 Hz, 1 H), 7.78 (s, 1 H), 8.26 (s, 1 H), 8.71 (s, 1 H), 10.91 (s br, 1 H), 11.50 (s, 1 H); HRMS calcd for $C_{16}H_{13}Cl_3N_4O_3Na$ 436.994 544 5, found 436.994 694 (M + Na), Dev = 0.34 ppm.

***N*-{4-Chloro-3-[3-(2,4-dichlorobenzoyl)ureido]phenyl}-acetamide (31).** 1-(5-Amino-2-chlorophenyl)-3-(2,4-dichlorobenzoyl)urea (100 mg, 0.28 mmol) (synthesis as described for **30**) was dissolved in 5 mL of *N*-methylpyrrolidone, which was warmed to 50 °C, and 22 mg (0.28 mmol) of acetyl chloride was added and the mixture heated to 50 °C for 15 min. After cooling to room temperature, the precipitate was filtered and washed with acetonitrile. The residue was purified by HPLC [acetonitrile/(H_2O + 0.1% trifluoroacetic acid) = 5/95 to 100/0, 15 min] to give 11 mg (10%) of **31**: ^{1}H NMR (500 MHz, DMSO-d_6) δ 2.07 (s, 3 H), 7.43 (d, J = 8.6 Hz, 1H), 7.55−7.60 (m, 2 H), 7.72 (d, J = 8.3 Hz, 1 H), 7.80 (s, 1 H), 8.46 (s, 1 H), 10.17 (s, 1 H), 10.90 (s br, 1 H), 11.56 (s, 1 H).

***N*-{3-[3-(2,4-Dichlorobenzoyl)ureido]-4-methoxyphenyl}acetamide (32). 29** (100 mg, 0.28 mmol) was dissolved in 5 mL of *N*-methylpyrrolidone, which was warmed to 50 °C, 22 mg (0.28 mmol) of acetyl chloride was added, and the mixture heated to 50 °C for 15 min. After cooling to room temperature, the precipitate was filtered and washed with acetonitrile. The residue was purified by HPLC [acetonitrile/(H_2O + 0.1% trifluoroacetic acid) = 5/95 to 100/0, 15 min] to give 7 mg (6%) of **32**: ^{1}H NMR (500 MHz, DMSO-d_6) δ 2.01 (s, 3 H), 3.85 (s, 3H), 7.02 (d, J = 9.2 Hz, 1H), 7.47 (dd, J = 8.3 Hz, J = 2.2 Hz, 1H), 7.57 (d, J = 7.7 Hz, 1 H), 7.68 (d, J = 8.3 Hz, 1H), 7.75 (s, 1 H), 8.39 (s, 1 H), 9.85 (s, 1 H), 10.76 (s br, 1 H), 11.33 (s, 1 H); HRMS calcd for $C_{17}H_{15}Cl_2N_3O_4Na$ 418.033 182 5, found 418.033 503 (M + Na), Dev = 0.77 ppm.

4-[3-(2,4-Dichlorobenzoyl)ureido]-3-methoxy-*N*-methylbenzamide (33). To a suspension of 200 mg (1.05 mmol) of 2,4-dichlorobenzamide in 10 mL of 1,2 dichloroethane was added 140 μL (1.63 mmol) of oxalyl dichloride and the mixture heated to reflux for 16 h. The solvent was removed in vacuo and 2 mL of toluene was added. Evaporation twice in vacuo removed the oxalyl dichloride. The residue was dissolved in 5 mL of acetonitrile, a solution of 95 mg (0.53 mmol) 4-amino-3-methoxy-*N*-methyl-benzamide in 5 mL of acetonitrile was added, and the mixture refluxed for 4 h. After cooling to room temperature, 3 mL of acetonitrile was added and the precipitate was filtered and washed with acetonitrile to give 176 mg (84%) of **33**: mp 187−189 °C; ^{1}H NMR (300 MHz, DMSO-d_6) δ 2.79 (d, J = 4.7 Hz, 3 H), 3.95 (s, 3 H), 7.46−7.70 (m, 4 H) 8.24 (d, J = 8.3 Hz, 1 H), 8.41 (q, J = 4.7 Hz, 1 H); HRMS calcd for $C_{17}H_{15}Cl_2N_3O_4Na$ 418.033 182 5, found 418.033 381 (M + Na), Dev = 0.48 ppm.

4-[3-(2-Chloro-4-fluorobenzoyl)ureido]-2-hydroxy-5-methoxybenzoic Acid (34). To a suspension of 379 mg (2.18 mmol) of 2-chloro-4-fluorobenzamide in 16 mL of 1,2-dichloroethane was added 281 μL (3.27 mmol) of oxalyl dichloride and the mixture heated to reflux for 21 h. The solvent was removed in vacuo and 5 mL of toluene was added. Evaporation in vacuo removed the oxalyl dichloride. The residue was dissolved in 7 mL of acetonitrile and added to a solution of 200 mg (1.09 mmol) of 4-amino-2-hydroxy-5-methoxybenzoic acid and 222 μL (1.09 mmol) of bis(trimethylsilyl)acetamide in 7 mL of acetonitrile, and the reaction mixture was refluxed for 4 h. After cooling to 0 °C, the precipitate was filtered and washed with ethanol give 326 mg (78%) of **34**: mp 256−257 °C; ^{1}H NMR (300 MHz, DMSO-d_6) δ 3.87 (s, 3 H), 7.31 (s, 1 H), 7.37 (td, J = 8.6 Hz, J = 2.7 Hz, 1 H), 7.61 (dd, J = 8.9 Hz, J = 2.6 Hz, 1 H), 7.73 (dd, J = 8.6 Hz, J = 6.0 Hz, 1 H), 7.87 (s, 1 H), 11.09 (s br, 2 H), 11.45 (s br, 1 H); HRMS calcd for $C_{16}H_{12}ClFN_2O_6Na$ 405.026 0131, found 405.026 241 (M + Na), Dev = 0.56 ppm.

4-[3-(2-Chloro-4,5-difluorobenzoyl)ureido]-2-hydroxy-5-methoxybenzoic Acid (35). To a suspension of 420 mg (2.18 mmol) of 2-chloro-4,5-difluorobenzamide in 16 mL of 1,2-dichloroethane was added 281 μL (3.27 mmol) of oxalyl dichloride and the mixture heated to reflux for 21 h. The solvent was removed in vacuo and 5 mL of toluene was added. Evaporation in vacuo removed the oxalyl dichloride. The residue was dissolved in 7 mL of acetonitrile and added to a solution of 200 mg (1.09 mmol) of 4-amino-2-hydroxy-5-methoxybenzoic acid and 222 μL (1.09 mmol) of bis(trimethylsilyl)acetamide in 7 mL of acetonitrile, and the reaction mixture was refluxed for 4 h. After addition of 0.3 mL of methanol and cooling to 0 °C, the precipitate was filtered and washed with ethanol to give 386 mg (84%) of **35**: mp 249−251 °C; ^{1}H NMR (300 MHz, DMSO-d_6) δ 3.88 (s, 3 H), 7.34 (s, 1 H), 7.84−7.98 (m, 3 H), 11.01 (s br, 1 H), 11.15 (s br, 1 H), 11.52 (s br, 1 H), 13.80 (s br, 1 H); HRMS calcd for $C_{16}H_{11}ClF_2N_2O_6Na$ 423.016 591 3, found 423.016 838 (M + Na), Dev

= 0.58 ppm. Anal. Calcd ($C_{16}H_{11}ClF_2N_3O_6$): C, 47.96; H, 2.77; N, 6.99. Found: C, 47.91; H, 2.88; N, 7.09.

1-(2-Chloro-4-fluorobenzoyl)-3-(4-hydroxymethyl-2-methoxyphenyl)urea (36). To a suspension of 96 mg (0.63 mmol) of (4-amino-3-methoxyphenyl)methanol in 10 mL of acetonitrile was added a solution of 138 mg (0.69 mmol) of 2-chloro-4-fluorobenzoyl isocyanate (synthesis as described for **18**) in 0.6 mL of dichloromethane and the mixture stirred at room temperature for 1 h. The precipitate was filtered, washed with acetonitrile, and purified by liquid chromatography using silica gel and dichloromethane/methanol = 100/1.5 as eluent to give 30 mg (7%) of (2-chloro-4-fluorobenzoyl)carbamic acid 4-[3-(2-chloro-4-fluorobenzoyl)ureido]-3-methoxybenzyl ester as a byproduct and 50 mg (23%) of **36**: ^{1}H NMR (300 MHz, DMSO-d_6) δ 3.90 (s, 3 H), 4.50 (d, J = 6.4 Hz, 2 H), 5.17 (t, J = 6.4 Hz, 1 H), 6.91 (d, J = 8.8 Hz, 1 H), 7.16 (s, 1 H), 7.35 (t, J = 9.8 Hz, 1 H), 7.60 (d, J = 8.8 Hz, 1 H), 7.74 (dd, J = 9.8 Hz, J = 7.8 Hz, 1 H), 8.13 (d, J = 7.8 Hz, 1 H), 10.78 (s br, 1 H), 11.25 (s br, 1 H); HRMS calcd for $C_{16}H_{14}ClFN_2O_4Na$ 375.051 833 9, found 375.052 049 (M + Na), Dev = 0.57 ppm.

4-[3-(2-Bromobenzoyl)ureido]-3-methoxybenzoic Acid (37). 4-Amino-3-methoxybenzoic acid *tert*-butyl ester (100 mg, 0.45 mmol) in 8 mL of dichloromethane/saturated aqueous $NaHCO_3$ solution = 1/1 was stirred at 0 °C, and 110 μL of a 20% solution of phosgene in toluene was added. After 15 min of stirring at room temperature, the aqueous layer was separated and extracted three times with dichloromethane. The combined organic layers were dried with Na_2SO_4 and evaporated in vacuo to give 180 mg of 4-isocyanato-3-methoxybenzoic acid *tert*-butyl ester. To a solution of 64 mg (0.32 mmol) of 2-bromobenzamide in 3 mL of xylene was added 80 mg (0.32 mmol) of the isocyanate. The reaction mixture was stirred at 120 °C for 3 h. The solvent was evaporated in vacuo and the residue was purified by HPLC [acetonitrile/(H_2O + 0.1% trifluoroacetic acid) = 5/95 to 100/0, 15 min] to give 4-[3-(2-bromobenzoyl)ureido]-3-methoxybenzoic acid *tert*-butyl ester. This material was dissolved in 5 mL of dichloromethane and 0.5 mL of trifluoroacetic acid was added. The solvent was evaporated in vacuo and the residue was purified by HPLC [acetonitrile/(H_2O + 0.1% trifluoroacetic acid) = 5/95 to 100/0, 15 min] to give 16 mg (14%) of **37**: mp 285−287 °C; ^{1}H NMR (300 MHz, DMSO-d_6) δ 3.96 (s, 1 H), 7.44−7.64 (m, 5 H), 7.72 (d, J = 7.3 Hz, 1 H), 8.32 (d, J = 9.2 Hz, 1 H), 11.08 (s, 1 H), 11.40 (s, 1 H); HRMS calcd for $C_{16}H_{13}BrN_2O_5Na$ 414.990 005 2, found 414.990 366 (M + Na), Dev = 0.87 ppm.

5-Chloro-4-[3-(2-chloro-4,5-difluorobenzoyl)ureido]-2-hydroxybenzoic Acid (38). To a suspension of 695 mg (3.63 mmol) of 2-chloro-4,5-difluorobenzamide in 25 mL of 1,2-dichloroethane was added 466 μL (5.43 mmol) of oxalyl dichloride and the mixture heated to reflux for 22 h. The solvent was removed in vacuo and 5 mL of toluene was added. Evaporation in vacuo removed the oxalyl dichloride. The residue was dissolved in 13 mL of acetonitrile and added to a solution of 340 mg (1.81 mmol) of 4-amino-5-chloro-2-hydroxybenzoic acid and 368 μL (1.81 mmol) of bis(trimethylsilyl)-acetamide in 13 mL of acetonitrile, and the reaction mixture was refluxed for 4.5 h. After addition of 0.3 mL of methanol and cooling to 0 °C, the precipitate was filtered, washed with ethanol, and dried in vacuo to give 477 mg (65%) of **38**: mp 250−253 °C dec; ^{1}H NMR (300 MHz, DMSO-d_6) δ 2.07 (acetonitrile), 7.86 (s, 1 H), 7.88−7.99 (m, 3 H), 11.12 (s br, 1 H), 11.40 (s br, <1 H), 11.70 (s br, 1 H); HRMS calcd for $C_{15}H_8Cl_2F_2N_2O_5Na$ 426.967 054 3, found 426.967 292 (M + Na), Dev = 0.56 ppm.

4-[3-(2-Chloro-4,5-difluorobenzoyl)ureido]-3-(2,2,2-trifluoroethoxy)benzoic Acid (39). To a suspension of 86 mg (0.45 mmol) of 2-chloro-4,5-difluorobenzamide in 10 mL of 1,2-dichloroethane was added 54 μL (0.63 mmol) of oxalyl dichloride and the mixture heated to reflux for 18 h. The solvent was removed in vacuo and 5 mL of toluene was added. Evaporation twice in vacuo removed the oxalyl dichloride. The residue was dissolved in 6 mL of acetonitrile, a heated solution of 53 mg (0.23 mmol) of 4-amino-3-(2,2,2-trifluoroethoxy)-benzoic acid in 2 mL of acetonitrile was added, and the mixture refluxed for 3 h. After cooling to room temperature, the solvent was evaporated and the residue was purified by HPLC [acetonitrile/(H_2O + 0.1% trifluoroacetic acid) = 5/95 to 100/0, 15 min] to give 2.6 mg (3%) of **39**: ^{1}H NMR (300 MHz, DMSO-d_6) δ 5.00 (q, J = 8.6 Hz, 2 H), 7.68−7.71 (m, 1 H), 7.71 (s, 1 H), 7.87−7.98 (m, 2 H), 8.37 (d, J = 9.0 Hz, 1 H), 11.08 (s br, 1 H), 11.53 (s br, 1 H), 12.93 (s br, 1 H); MS (ES) m/z: 451.1/453.0 (M − H)$^-$.

***N*-{4-Chloro-3-[3-(2-chloro-4,5-difluorobenzoyl)ureido]-phenyl}acetamide (40).** To a suspension of 12.0 g (62.60 mmol) of 2-chloro-4,5-difluorobenzamide in 50 mL of dichloromethane was added 15.9 g (0.13 mol) of oxalyl dichloride and the mixture heated to reflux for 24 h. The solvent was removed in vacuo and 50 mL of toluene was added. Evaporation twice in vacuo removed the oxalyl dichloride to give 12 g of 2-chloro-4,5-difluorobenzoyl isocyanate as an oil. The isocyanate (1.26 g, 5.8 mmol) was added to a solution of 1.00 g (5.8 mmol) of 2-chloro-5-nitrophenylamine in 2 mL of *N*-methylpyrrolidone and the mixture stirred for 30 min. Then, 2 mL of water was added to the reaction mixture and the precipitate was filtered and washed with water to give 2.2 g (97%) of 1-(2-chloro-5-nitrophenyl)-3-(2-chloro-4,5-difluorobenzoyl)urea. 1-(2-Chloro-5-nitrophenyl)-3-(2-chloro-4,5-difluorobenzoyl)urea (2.2 g, 5.5 mmol) was suspended in 30 mL of ethyl acetate and heated to 70 °C. $SnCl_2{\cdot}H_2O$ (6.34 g, 28.2 mmol) was added and the reaction mixture was stirred at 70 °C for 5 h. After cooling to room temperature, the reaction mixture was basified to pH 8 with 2 N NaOH, and the reaction mixture was extracted with dichloromethane. The organic layer was dried with $MgSO_4$ and evaporated in vacuo to give 1.39 g (69%) of 1-(5-amino-2-chlorophenyl)-3-(2-chloro-4,5-difluorobenzoyl)urea. 1-(5-Amino-2-chlorophenyl)-3-(2-chloro-4,5-difluorobenzoyl)urea (100 mg, 0.28 mmol) was dissolved in 1.5 mL of *N*-methylpyrrolidone, 32 mg (0.31 mmol) of acetic acid anhydride was added, and the mixture heated to 60 °C for 30 min. After cooling to room temperature, 2 mL of water was added and the precipitate was filtered and washed with water. The residue was purified by HPLC [acetonitrile/(H_2O + 0.1% trifluoroacetic acid) = 5/95 to 100/0, 15 min] to give 34 mg (31%) of **40**: ^{1}H NMR (500 MHz, DMSO-d_6) δ 2.05 (s, 3 H), 7.45 (d, J = 8.9 Hz, 1 H), 7.56 (dd, J = 8.9 Hz, J = 2.5 Hz, 1 H), 7.87−7.98 (m, 2 H), 8.48 (d, J = 2.5 Hz, 1 H), 10.15 (s, 1 H), 10.85 (s br, 1 H), 11.56 (s, 1 H); HRMS calcd for $C_{16}H_{11}Cl_2F_2N_3O_3Na$ 424.003 774 1, found 424.003 953 (M + Na), Dev = 0.42 ppm.

***N*-{3-[3-(2-Chloro-4,5-difluorobenzoyl)ureido]-4-methoxyphenyl}acetamide (41).** 2-Chloro-4,5-difluorobenzoyl isocyanate (1.29 g, 5.9 mmol) (synthesis as described for **40**) was added to a solution of 1.00 g (5.9 mmol) of 2-methoxy-5-nitrophenylamine in 2 mL of *N*-methylpyrrolidone and the mixture stirred for 1 h. Water (2 mL) was added to the reaction mixture and the precipitate was filtered and washed with water to give 2.2 g (97%) of 1-(2-chloro-4,5-difluorobenzoyl)-3-(2-methoxy-5-nitrophenyl)urea. 1-(2-Methoxy-5-nitrophenyl)-3-(2-chloro-4,5-difluorobenzoyl)urea (2.2 g, 5.7 mmol) was suspended in 50 mL of ethyl acetate and heated to 70 °C. $SnCl_2{\cdot}H_2O$ (6.42 g, 28.5 mmol) was added and the reaction mixture was stirred at 70 °C for 1 h. After cooling to room temperature, the reaction mixture was basified to pH 8 with 2 N NaOH. The organic layer was washed with water, dried with Na_2SO_4, and evaporated in vacuo to give 1.4 g (69%) of 1-(5-amino-2-methoxyphenyl)-3-(2-chloro-4,5-difluorobenzoyl)urea as an oil. 1-(5-Amino-2-methoxyphenyl)-3-(2-chloro-4,5-difluorobenzoyl)-urea (100 mg, 0.28 mmol) was dissolved in 1 mL of *N*-methylpyrrolidone, 29 mg (0.28 mmol) of acetic acid anhydride was added, and the mixture stirred for 2 h. The reaction mixture was separated between ethyl acetate and water. The organic layer was dried with Na_2SO_4 and evaporated in vacuo. The residue was purified by HPLC [acetonitrile/(H_2O + 0.1% trifluoroacetic acid) = 5/95 to 100/0, 15 min] to give 27 mg (24%) of **41**: ^{1}H NMR (500 MHz, DMSO-d_6) δ 2.01 (s, 3 H), 3.87 (s, 3 H), 7,01 (d, J = 8.9 Hz, 1 H), 7.48 (dd, J = 8.9 Hz, J = 2.8 Hz, 1 H), 7.86−7.96 (m, 2 H), 8.31 (d, J = 2.8 Hz, 1 H), 9.85 (s, 1 H), 10.75 (s br, 1 H), 11.35 (s, 1 H); HRMS calcd

for $C_{17}H_{14}ClF_2N_3O_4Na$ 420.053 311 2, found 420.053 454 (M + Na), Dev = 0.34 ppm.

1-{3-[3-(2-Chloro-4,5-difluorobenzoyl)ureido]-4-methoxyphenyl}-3-methylurea (42). To a solution of 600 mg (1.70 mmol) of 1-(5-amino-2-methoxyphenyl)-3-(2-chloro-4,5-difluorobenzoyl)urea (synthesis as described for **41**) in 5 mL of acetonitrile was added 69 mg (1.70 mmol) of isocyanatomethane and the mixture stirred for 1 h. The precipitate was filtered and washed with acetonitrile to give 638 mg (91%) of **42**: ^{1}H NMR (400 MHz, DMSO-d_6) δ 2.63 (d, J = 4.7 Hz, 3 H), 3.83 (s, 3 H), 5.80 (q br, J = 4.7 Hz, 1 H), 6.95 (d, J = 9.0 Hz, 1 H), 7.29 (dd, J = 9.0 Hz, J = 2.7 Hz, 1 H), 7.86−7.95 (m, 2 H), 8.10 (d, J = 2.5 Hz, 1 H), 8.40 (s, 1 H), 10.69 (s br, 1 H), 11.31 (s, 1 H); HRMS calcd for $C_{17}H_{15}ClF_2N_4O_4Na$ 435.064 210 2, found 435.064 414 (M + Na), Dev = 0.29 ppm.

1-(2-Chloro-4,5-difluorobenzoyl)-3-[2-methoxy-4-(5-methyl-4*H*-[1,2,4]triazol-3-yl)phenyl]urea (43). To a suspension of 1.0 g (5.2 mmol) of 2-chloro-4,5-difluorobenzamide in 5 mL of dichloromethane was added 690 μL (8.03 mmol) of oxalyl dichloride at 0 °C and the mixture heated to reflux for 6 h. The solvent was removed in vacuo and 3 mL of toluene was added. Evaporation twice in vacuo removed the oxalyl dichloride to give 1.13 g (quant.) of 2-chloro-4,5-difluorobenzoyl isocyanate. A solution of 293 mg (1.35 mmol) of the isocyanate in 2 mL of dichloromethane was added to a suspension of 275 mg (1.34 mmol) of 2-methoxy-4-(5-methyl-4*H*-[1,2,4]triazol-3-yl)phenylamine in 3 mL of acetonitrile and the mixture stirred at room temperature for 30 min. The precipitate was filtered, dissolved in dichloromethane/methanol, filtered again, and evaporated in vacuo. The residue was stirred with methyl *tert*-butyl ether and filtered to give 243 mg (43%) of **43**: mp 226.5−227.5 °C; ^{1}H NMR (300 MHz, DMSO-d_6) δ 2.41 (s, 3 H), 3.97 (s, 3 H), 7.60 (dd, J = 8.6 Hz, J = 1.7 Hz, 1 H), 7.64 (d, J = 1.7 Hz), 1 H), 7.87−7.97 (m, 2 H), 8.27 (d, J = 8.3 Hz, 1 H), 10.85 (s br, 1 H), 11.40 (s br, 1 H); HRMS calcd for $C_{18}H_{14}ClF_2N_5O_3Na$ 444.064 544 5, found 444.064 812 (M + Na), Dev = 0.60 ppm.

1-(2,4-Dichlorobenzoyl)-3-(1*H*-indol-6-yl)urea (44). To a suspension of 950 mg (5.00 mmol) of 2,4-dichlorobenzamide in 10 mL of 1,2-dichloro-ethane was added 600 μL (6.99 mmol) of oxalyl dichloride and the mixture heated to reflux for 14 h. The solvent was removed in vacuo and 5 mL of toluene was added. Evaporation twice in vacuo removed the oxalyl dichloride. The isocyanate (216 mg, 1.00 mmol) was dissolved in 10 mL of acetonitrile, 159 mg (1.20 mmol) of 6-aminoindole was added, and the mixture refluxed for 3 h. After cooling to room temperature, the precipitate was filtered and washed with acetonitrile to give 218 mg (52%) of **44**: ^{1}H NMR (300 MHz, DMSO-d_6) δ 6.40 (t, J = 1.5 Hz, 1 H), 6.96 (dd, J = 8.3 Hz, J = 1.9 Hz, 1 H), 7.30 (dd, J = 2.6 Hz, J = 3.8 Hz, 1 H), 7.49 (d, J = 9.0 Hz, 1 H), 7.57 (dd, J = 8.3 Hz, J = 2.6 Hz, 1 H), 7.68 (d, J = 9.0 Hz, 1 H), 7.78 (d, J = 1.9 Hz, 1 H), 7.87 (s, 1 H), 10.35 (s br, 1 H), 11.05 (s br, 1 H), 11.18 (s br, 1 H); MS (ES) m/z 346.1/348.1 $(M - H)^-$; HRMS calcd for $C_{16}H_{11}Cl_2N_3O_2Na$ 370.012 053 1, found 370.012 331 (M + Na), Dev = 0.75 ppm. Anal. Calcd ($C_{16}H_{11}Cl_2N_3O_2$): C, 55.19; H, 3.18; N, 12.07. Found: C, 55.03; H, 3.25; N, 12.05.

1-(2-Chloro-4-fluorobenzoyl)-3-(1,2,3,4-tetrahydroquinolin-7-yl)urea (45). To a suspension of 420 mg (2.42 mmol) of 2-chloro-4-fluorobenzamide in 17 mL of 1,2-dichloroethane was added 311 μL (3.62 mmol) of oxalyl dichloride and the mixture heated to reflux for 18 h. The solvent was removed in vacuo and 5 mL of toluene was added. Evaporation in vacuo removed the oxalyl dichloride. The residue was dissolved in 8 mL of acetonitrile and added to a solution of 300 mg (1.21 mmol) of 7-amino-3,4-dihydro-2*H*-quinoline-1-carboxylic acid *tert*-butyl ester and 246 μL (1.21 mmol) of bis(trimethylsilyl)-acetamide in 8 mL acetonitrile and the reaction mixture was refluxed for 4 h. The solvent was evaporated and the residue was purified by liquid chromatography using silica gel and ethyl acetate/heptane = 1/4 to 1/0 as eluent to give 130 mg (12%) of **45**: ^{1}H NMR (300 MHz, DMSO-d_6) δ 1.73−1.84 (m, 2 H), 2.66 (t, J = 6.7 Hz, 2 H), 3.18 (t, J = 6.7 Hz, 2 H), 6.58 (dd, J = 7.2 Hz, J = 1.9 Hz, 1 H), 6.78−6.83 (m, 2 H), 7.34 (td, J = 8.3 Hz, J = 3.0 Hz, 1 H), 7.58 (dd, J = 8.3 Hz, J = 1.9 Hz, 1 H), 7.69 (dd, J = 8.3 Hz, J = 7.2 Hz, 2 H), 10.15 (s br, 1 H), 10.80 (s br, 1 H), 11.09 (s br, 1 H); HRMS calcd for $C_{17}H_{15}ClFN_3O_2Na$ 370.072 903 7, found 370.073 194 (M + Na), Dev = 0.78 ppm.

Pharmacophore Generation. The pharmacophore has been generated with the HypoGen module in Catalyst 4.7 using a training set of 24 hlGPa inhibitors, with IC_{50} values ranging from 23 nM to 15 μM (see Table 1).[27] The chemical structures of all compounds in the training set were drawn in Maestro (Schrödinger Inc.). For each molecule, a conformational set was generated in Macromodel (Schrödinger Inc.)[28] by a Monte Carlo search using water as solvent (1000 iterations, MMFF force field).[29] All conformers within a 25 kJ/mol energy window from the global minimum were imported into Catalyst and used for pharmacophore generation. Catalyst (HypoGen module) allows a maximum of five features in pharmacophore generation. Therefore, all the features of the feature dictionary were first considered and subsequently reduced to a maximum of five. Initial runs revealed that one "hydrogen-bond-donor" and one "hydrogen-bond-acceptor" feature as well as several "hydrophobic" features mediate the biological activity at the target enzyme and were thus selected for the final hypothesis generation run. Catalyst considers and discards many thousands of models and selects the best hypotheses from many possibilities by applying a cost analysis.[30] For each model three cost values, expressed in bits, are assessed: the "null", the "fixed", and the "total" costs. The null and the fixed costs are dependent on the training data set, the features selected, and the run options. The fixed cost corresponds to the simplest model that fits all data perfectly, while the null cost corresponds to the model with no features and estimates activity as the average of the activity of the training set. To be statistically significant, one hypothesis should have a total cost close to the fixed cost and far from the null cost. The best pharmacophore hypothesis generated for the GP training set ("fixed" cost 80 bits, "total" cost 95 bits, "null" cost 147 bits) revealed a good correlation between predicted and observed activity (R = 0.9) and was thus selected for further analysis. The finding that the total costs were much closer to the fixed cost than to the null cost indicates that a significant model has been obtained. The difference between the "total" cost and "null" cost is 52, indicating a predictive correlation probability of 75−90%.

Generation of the 3D QSAR Model. The most critical point in the CoMFA procedure is the alignment of the molecules in Cartesian space. In this study, the above-described pharmacophore was used to generate the overall alignment of all 40 molecules within the training set (see Table 3). Therefore, the training set molecules were mapped onto the pharmacophore within Catalyst and imported into Sybyl6.9.[31] For all molecules, Gasteiger partial charges were calculated. A CoMFA table was built containing the biological data of the hlGPa assay ($-\log IC_{50}$, observed in Table 3). The CoMFA analysis was performed using separate columns for the electrostatic and the steric fields (electrostatic columns were kept within van der Waals sphere of molecules). The field regions were generated automatically and manually adapted to cover the area of all training set molecules (grid spacing 1 Å). The statistical analysis was carried out by applying the PLS procedure using the standard scaling method (COMFA_ST). Furthermore, an energy cutoff value of 30 kcal/mol was selected for the steric field. Cross-validated PLS runs were carried out to establish the optimal number of components to be used in the final fitting model. The final model has an optimal number of five components (selected on the basis of the minimum s_{cross} value criterion). The steric and electrostatic contributions to the final model were found to be 35% and 65%, respectively. The standard deviation of s = 0.22 (factor 1.7 in nonlogarithmic scale) is in the range of the experimental error within the hlGPa assay. The descriptive and predictive abilities are evaluated by the statistic parameters r^2 = 0.92 and s = 0.22, and q^2 = 0.66 and s_{cross} = 0.45, respectively.

Protein Crystallography. rabmGPb was isolated from rabbit skeletal muscle according to the procedure of Fischer and Krebs.[32] The complex of rabmGPb with **1** was cocrystallized as described by Zographos et al. using a 4-fold molar excess of inhibitor without addition of glucose.[7] Crystallographic data to 2.3 Å resolution were collected at room temperature from a single crystal on an image plate RAXIS IV using a Rigaku Ru−H3RHB belt drive rotating anode source and were processed with programs DENZO and SCALEPACK[33] (R_{sym} = 9.5%; 95.7% completeness; mean $I/\sigma(I)$ = 15.6; $I/\sigma(I)$ = 5.9 for 2.30−2.26 Å shell). Structure refinement was based on a model of room-temperature rabmGPb[34] and performed with the programs XPLOR[35] and O.[36] Iterative refinement of atom positions and restrained individual temperature factors resulted in an *R*-factor of 19.3% (R_{free} = 23.3%) and good geometric quality. The final model contains protein residues 13−314 and 324−837, 240 water molecules, and one pyridoxal phosphate molecule, which is covalently linked to the enzyme, as well as inhibitor **1**.

hlGPa was expressed and purified according to the procedures described by Rath et al.[4] For cocrystallization, the protein was concentrated to 20−30 mg/mL in a solution containing 10 mM NaBES (pH 6.8), 1 mM EDTA, and 5 mM DTT. After concentration, 50 mM glucose and 2 mM inhibitor **21** were added. The resulting solution was incubated at 4 °C for 2 h before hanging drops were set up by mixing equal volumes of the protein solution with a reservoir solution containing 100 mM NaMES (pH 6.0), 100 mM glucose, and 12.5% (w/v) MPD. Crystals were grown at 20 °C and flash frozen in liquid nitrogen directly from the crystallization drop. Crystallographic data were collected to 1.9 Å resolution at ESRF beamline ID-14 EH1. Crystals were of space group $P3_1$ ($a = b$ = 124.5 Å, c = 123.2 Å; $\alpha = \beta$= 90°; γ = 120°). Data processing was done in XDS,[37] providing good data quality (R_{sym} = 5.6%; 99.6% completeness; mean $I/\sigma(I)$ = 16.5; $I/\sigma(I)$ = 5.2 for 1.9−2.0 Å shell). The coordinates of PDB entry 1FC0[4] were used as a starting model for iterative refinement with programs CNX[38] and QUANTA,[39] resulting an *R*-factor of 23.2% (R_{free} = 25.6%) and good geometric quality. The final model contains two crystallographically independent chains of hlGPb (containing residues 23−249, 261−316, and 324−831 for chain A and residues 23−249, 261−316, and 324−831 for chain B) as well as 759 water molecules. Each chain is covalently linked to a pyridoxal phosphate molecule and contains one glucose molecule as well as one molecule of inhibitor **21**. Structures are illustrated with PyMOL.[40] The coordinates of the protein−inhibitor complexes have been deposited at the Protein Data Bank under accession codes 1WUT (complex structure of **1** with rabbit muscle phosphorylase b) and 2ATI (complex structure of **21** with human liver glycogen phosphorylase a).

Glycogen Phosphorylase Activity. The activity of recombinant hlGPa was monitored in the direction of glycogen synthesis in an assay mixture (100 μL final volume) that contained 30 mM HEPES, pH 7.2, 60 mM KCl, 1.5 mM EDTA, 1.5 mM $MgCl_2$, 1 mg/mL glycogen, 1 mM glucose-1-phosphate, 7 mU hlGPa, 1% DMSO, and the respective inhibitors at a concentration within the range 0−100 μM. The reaction was initiated by the addition of glucose-1-phosphate and incubated for 40 min at 25 °C. The inorganic phosphate released was assayed according to Drueckes et al.[41] The activity of the enzyme in the direction of glycogen breakdown was measured by the photometrical determination at 340 nm of the rate of NADPH formation in a mixture that contained 45 mM HEPES, pH 6.8, 5 mM potassium phosphate, 100 μM EDTA, 15 mM $MgCl_2$, 4 μM glucose 1,6-bisphosphate, 0.34 μM NADP, 1 mg/mL glycogen, 1% DMSO, 1 U/mL hlGPa, 6 U/mL phosphoglucomutase, and 2 U/mL glucose-6-phosphate dehydrogenase.

RabmGP activity for compound **21** was measured in the direction of glycogen synthesis with 10 μg/mL enzyme at constant concentrations of glycogen (1% w/v), 4 mM glucose-1-phosphate, 40 μM AMP, and various concentrations of inhibitor **21** (1−15 μM) as described previously.[10]

Glucagon-Induced Glycogenolysis in Primary Hepatocytes. Primary hepatocytes, isolated from adult male Sprague−Dawley rats (Moellgaard, Lille, Skensved, Denmark) fed ad libitium essentially as described, were seeded into 96-well plates.[42] After attachment, the cells were incubated overnight with William's E-Medium, supplemented with 25 mM glucose and 100 nM insulin, to accumulate glycogen stores. The cells were washed three times with prewarmed, oxygen-saturated KHH (20 mM HEPES, 115 mM NaCl, 4.5 mM KCl, 4.5 mM $CaCl_2$, 1.1 mM KH_2PO_4, 1.1 mM $MgSO_4$, pH 7.4) and subsequently incubated for 30 min at 37 °C in a final volume of 100 μL in KHH, 1% DMSO, and the respective inhibitor at a concentration within the range 0−100 μM (inclusion of 1% DMSO was shown not to affect the extent of glucagon-induced glycogenolysis). Glycogenolysis was initiated by the addition of 10 μL of glucagon (final concentration 10 nM). Medium (10 μL) was removed immediately before and 90 min after the addition of glucagon, and glucagon-induced glucose release into the medium was determined using the Amplex Red Glucose Assay Kit (Molecular Probes), according to the manufacturer's instructions.

Glucagon-Induced Glycogenolysis in Anaesthetized Rats. Blood glucose levels were assayed in anaesthetized male Wistar rats (HsdCpb:WU) as described previously.[43] Rats had free access to food and water until the start of the study. Rats were anaesthetized with an intraperitoneal injection of pentobarbital sodium (60 mg/kg) and tracheotomized, and one jugular vein per rat was cannulated for intravenous infusion. Anaesthesia was maintained for up to 6 h by subcutaneous infusion of pentobarbital sodium (adjusted to the anaesthetic depth of the individual animal, about 24 mg/kg/h). Body temperature was monitored with a rectal probe thermometer, and temperature was maintained at 37 °C by means of a heated surgical table. Blood samples for glucose analysis (10 μL) were obtained from the tip of the tail every 15 min. The rats were allowed to stabilize their blood glucose levels after surgery for about 2 h. To investigate the effect of the test compound on the process of glycogenolysis, normal fed rats, having high amounts of liver glycogen, were used. During this study, glycogenolysis was induced by an intravenous bolus injection of glucagon at a dose of 1 mg/rat. It can be assumed that the hyperglycemia induced by the glucagon injection, which lasted about 120 min, was the result of the glucagon-induced breakdown of hepatic glycogen.

Acknowledgment. We thank Nicole Hörl, Michael Bauer, Nikolai Wöllmer, Herbert Weber, Wolfgang Röhner, Peter-Michael Blohm, and Detlev Schneider for their excellent technical support in the chemical synthesis of the described compounds. We acknowledge financial support from the Greek GRST (PENED-204/2001 to N.G.O.). We also wish to thank Marion Meyer, Anke Müller-Seeland, and Marion Stein for conducting the in vitro and in vivo compound profiling. The assistance of Paulette Bichet and Cecile Capdevila in protein production and of Katerina Tsitsanou, Matthias Dreyer, and Petra Loenze in protein crystallography is gratefully acknowledged.

Supporting Information Available: Table providing results from purity analyses by elemental analyses and HPLC for key target compounds, NMR data of compound **1**, and NMR spectra for selected compounds (**4**, **7**, **13**, **18**, **21**, **23**, **31**, **39**, **41**, and **42**). This material is available free of charge via the Internet at http://pubs.acs.org.

References

(1) Kenny, S. J.; Aubert, R. E.; Geiss, L. S. In *Diabetes in America*, 2nd ed.; Harris, M., Ed. Barthedsa, MD, 1995; pp 47−67.
(2) Landau, B. R.; Wahren, J.; Chandramouli, V.; Schumann, W. C.; Ekberg, K.; Kalhan, S. C. Contributions of gluconeogenesis to glucose production in the fasted state. *J. Clin. Invest.* **1996**, *98*, 378−385.

(3) Treadway, J. L.; Mendys, P.; Hoover, D. J. Glycogen phosphorylase inhibitors for treatment of type 2 diabetes mellitus. *Expert. Opin. Invest. Drugs* **2001**, *10*, 439−454.
(4) Rath, V. L.; Ammirati, M.; LeMotte, P. K.; Fennell, K. F.; Mansour, M. N.; Danley, D. E.; Hynes, T. R.; Schulte, G. K.; Wasilko, D. J.; Pandit, J. Activation of human liver glycogen phosphorylase by alteration of the secondary structure and packing of the catalytic core. *Mol. Cell* **2000**, *6*, 139−148.
(5) Newgard, C. B.; Hwang, P. K.; Fletterick, R. J. The family of glycogen phosphorylases: Structure and function. *Crit Rev. Biochem. Mol. Biol.* **1989**, *24*, 69−99.
(6) Gregoriou, M.; Noble, M. E.; Watson, K. A.; Garman, E. F.; Krulle, T. M.; de la, F. C.; Fleet, G. W.; Oikonomakos, N. G.; Johnson, L. N. The structure of a glycogen phosphorylase glucopyranose spirohydantoin complex at 1.8 A resolution and 100 K: The role of the water structure and its contribution to binding. *Protein Sci.* **1998**, *7*, 915−927.
(7) Zographos, S. E.; Oikonomakos, N. G.; Tsitsanou, K. E.; Leonidas, D. D.; Chrysina, E. D.; Skamnaki, V. T.; Bischoff, H.; Goldmann, S.; Watson, K. A.; Johnson, L. N. The structure of glycogen phosphorylase b with an alkyldihydropyridine-dicarboxylic acid compound, a novel and potent inhibitor. *Structure* **1997**, *5*, 1413−1425.
(8) Lu, Z.; Bohn, J.; Bergeron, R.; Deng, Q.; Ellsworth, K. P.; Geissler, W. M.; Harris, G.; McCann, P. E.; McKeever, B.; Myers, R. W.; Saperstein, R.; Willoughby, C. A.; Yao, J.; Chapman, K. A new class of glycogen phosphorylase inhibitors. *Bioorg. Med. Chem. Lett.* **2003**, *13*, 4125−4128.
(9) Kristiansen, M.; Andersen, B.; Iversen, L. F.; Westergaard, N. Identification, synthesis, and characterization of new glycogen phosphorylase inhibitors binding to the allosteric AMP site. *J. Med. Chem.* **2004**, *47*, 3537−3545.
(10) Oikonomakos, N. G.; Schnier, J. B.; Zographos, S. E.; Skamnaki, V. T.; Tsitsanou, K. E.; Johnson, L. N. Flavopiridol inhibits glycogen phosphorylase by binding at the inhibitor site. *J. Biol. Chem.* **2000**, *275*, 34566−34573.
(11) Oikonomakos, N. G.; Skamnaki, V. T.; Tsitsanou, K. E.; Gavalas, N. G.; Johnson, L. N. A new allosteric site in glycogen phosphorylase b as a target for drug interactions. *Structure. Fold. Des.* **2000**, *8*, 575−584.
(12) Rath, V. L.; Ammirati, M.; Danley, D. E.; Ekstrom, J. L.; Gibbs, E. M.; Hynes, T. R.; Mathiowetz, A. M.; McPherson, R. K.; Olson, T. V.; Treadway, J. L.; Hoover, D. J. Human liver glycogen phosphorylase inhibitors bind at a new allosteric site. *Chem. Biol.* **2000**, *7*, 677−682.
(13) Hoover, D. J.; Lefkowitz-Snow, S.; Burgess-Henry, J. L.; Martin, W. H.; Armento, S. J.; Stock, I. A.; McPherson, R. K.; Genereux, P. E.; Gibbs, E. M.; Treadway, J. L. Indole-2-carboxamide inhibitors of human liver glycogen phosphorylase. *J. Med. Chem.* **1998**, *41*, 2934−2938.
(14) Martin, W. H.; Hoover, D. J.; Armento, S. J.; Stock, I. A.; McPherson, R. K.; Danley, D. E.; Stevenson, R. W.; Barrett, E. J.; Treadway, J. L. Discovery of a human liver glycogen phosphorylase inhibitor that lowers blood glucose in vivo. *Proc. Natl. Acad. Sci. U.S.A.* **1998**, *95*, 1776−1781.
(15) Oikonomakos, N. G.; Chrysina, E. D.; Kosmopoulou, M. N.; Leonidas, D. D. Crystal structure of rabbit muscle glycogen phosphorylase a in complex with a potential hypoglycaemic drug at 2.0 A resolution. *Biochim. Biophys. Acta* **2003**, *1647*, 325−332.
(16) Weikert, R. J.; Bingham, S., Jr; Emanuel, M. A.; Fraser-Smith, E. B.; Loughhead, D. G.; Nelson, P. H.; Poulton, A. L. Synthesis and anthelmintic activity of 3′-benzoylurea derivatives of 6-phenyl-2,3,5,6-tetrahydroimidazo[2,1-*b*]thiazole. *J. Med. Chem.* **1991**, *34*, 1630−1633.
(17) Speziale, A. J.; Smith, L. R.; Fedder, J. E. The reaction of oxalyl chloride with amides. IV. Synthesis of Acyl Isocyanates. *J. Org. Chem.* **1965**, *30*, 4306−4307.
(18) Speziale, A. J.; Smith, L. R. The reaction of Oxalyl Chloride with Amides. II. Oxazolidindiones and Acylisocyanates. *J. Org. Chem.* **1963**, *28*, 1805−1811.
(19) Schroth, W.; Krieg, R.; Kluge, H.; Gaebler, M. Synthesis of aromatic acylisocyanates by thermolysis of 1,1-diacyl-3,3-dialkylureas. *Z. Chem.* **1985**, *25*, 398−399.
(20) Wiley, P. F. The reaction of amides with isocyanates. *J. Am. Chem. Soc.* **1949**, 1310−1311.
(21) Defossa, E.; Kadereit, D.; Schoenafinger, K.; Klabunde, T.; Burger, H.-J.; Herling, A.; Wendt, K.-U.; Von Roedern, E.; Enhsen, A.; Rieke-Zapp, J. Preparation of 4-(benzoylureido)-benzoic acids as antidiabetics, WO2003084922.
(22) Schoenafinger, K.; Defossa, E.; Kadereit, D.; Von Roedern, E.; Klabunde, T.; Burger, H.-J.; Herling, A.; Wendt, K.-U. Preparation of heterocyclylbenzoylureas for treating type 2 diabetes. WO2004007455.
(23) Defossa, E.; Kadereit, D.; Klabunde, T.; Burger, H.-J.; Herling, A.; Wendt, K.-U.; Von Roedern, E.; Schoenafinger, K. Preparation of N-[(phenylamino)carbonyl]benzamides as glycogen-phosphorylase-A inhibitors for the treatment of diabetes. WO2004007437.
(24) Defossa, E.; Kadereit, D.; Klabunde, T.; Burger, H.-J.; Herling, A.; Wendt, K.-U.; Von Roedern, E.; Schoenafinger, K.; Enhsen, A. Method for the production of carbonylamino substituted acyl phenyl urea derivatives, and use thereof in treating type 2 diabetes. WO2004065356.
(25) The limitation of a 3D pharmacophore model is that it does not capture electrostatic interactions in a quantitative manner, e.g. charge-supported hydrogen bonds are not distinguished from normal hydrogen bonds. Also repulsive electrostatic interactions are not taken into account for pharmacophore-based predictions of biological activity. Using the 3D pharmacophore for a quantitative prediction of the biological activity for the indole compound **44**, the tetrahydrochinolin compound **45**, and compound **28** (Y5 NO_2 group) is thus not possible. 3D QSAR models are necessary to capture electrostatic and hydrophobic interactions in a quantitative manner and have been used in addition to the 3D pharmacophore to guide the chemical optimization.
(26) Kruszynska, Y. T. Normal metabolism: The physiology of fuel homeostasis. In *Textbook of Diabetes;* Pickup, J. C., Williams, G., Eds.; 2nd ed.; Blackwell Sciences: Oxford, 1998; Volume 1, pp 11.1−11.37. *Textbook of Diabetes*, 2nd ed.; Pickup, J. C. W. G. e., Ed.; Blackwell Sciences: Oxford, 2005; pp 1−37.
(27) Catalyst, version 4.7; Accelrys Inc.: San Diego, CA, 2002.
(28) Mohamadi, F.; Richards, N. G. J.; Guida, W. C.; Liskamp, R.; Lipton, M.; Caufield, C.; Chang, G.; Hendrickson, T.; Still, W. C. Macromodel-An Integrated Software System for Modeling Organic and Bioorganic Molecules using Molecular Mechanics. *J. Comput. Chem.* **1990**, *11*, 440−445.
(29) Halgren, T. A. MMFF VII. Characterization of MMFF94, MMFF94s, and other widely available force fields for conformational energies and for intermolecular-interaction energies and geometries. *J. Comput. Chem.* **1999**, *20*, 730−738.
(30) For cost analysis, see Catalyst 4.7 documentation at www.accelrys.com/doc/life/catalyst47/help/HypoGenAlgRef.doc.html.
(31) SYBYL, version 6.9; Tripos, Inc.: St. Louis, MO, 2003.
(32) Fischer, E. H.; Krebs, E. G. Muscle phosphorylase b. *Methods Enzymol.* **1962**, *5*, 369−372.
(33) Otwinowski, Z.; Minor, W. Processing of X-ray diffraction data collected in oscillation mode. *Methods Enzymol.* **1997**, 307−326.
(34) Oikonomakos, N. G. unpublished results. 2004.
(35) Brunger, A. T. *X-PLOR: version 3.8, a system for protein crystallography and NMR. 2004;* Yale University Press: New Haven, CT.
(36) Jones, T. A.; Zou, J. Y.; Cowan, S. W. Kjeldgaard Improved methods for building protein models in electron density maps and the location of errors in these models. *Acta Crystallogr. A* **1991**, *47* (Pt 2), 110−119.
(37) Kabsch, W. Automatic processing of rotation diffraction data from crystals of initially unknown symmetry and cell constants. *J. Appl. Crystallogr.* **2004**, *26*, 795−800.
(38) Brunger, A. T.; Adams, P. D.; Clore, G. M.; DeLano, W. L.; Gros, P.; Grosse-Kunstleve, R. W.; Jiang, J. S.; Kuszewski, J.; Nilges, M.; Pannu, N. S.; Read, R. J.; Rice, L. M.; Simonson, T.; Warren, G. L. Crystallography & NMR system: A new software suite for macromolecular structure determination. *Acta Crystallogr. D. Biol. Crystallogr.* **1998**, *54* (Pt 5), 905−921.
(39) Quanta: Molecular Simulations Inc., San Diego, CA.
(40) PyMOL at http://www.pymol.org.
(41) Drueckes, P.; Schinzel, R.; Palm, D. Photometric microtiter assay of inorganic phosphate in the presence of acid-labile organic phosphates. *Anal. Biochem.* **1995**, *230*, 173−177.
(42) Schwab, D.; Herling, A. W.; Hemmerle, H.; Schubert, G.; Hagenbuch, B.; Burger, H. J. Hepatic uptake of synthetic chlorogenic acid derivatives by the organic anion transport proteins. *J. Pharmacol. Exp. Ther.* **2001**, *296*, 91−98.
(43) Herling, A. W.; Burger, H. J.; Schwab, D.; Hemmerle, H.; Below, P.; Schubert, G. Pharmacodynamic profile of a novel inhibitor of the hepatic glucose-6-phosphatase system. *Am. J. Physiol.* **1998**, *274*, G1087−G1093.
(44) Ekstrom, J. L.; Pauly, T. A.; Carty, M. D.; Soeller, W. C.; Culp, J.; Danley, D. E.; Hoover, D. J.; Treadway, J. L.; Gibbs, E. M.; Fletterick, R. J.; Day, Y. S.; Myszka, D. G.; Rath, V. L. Structure−activity analysis of the purine binding site of human liver glycogen phosphorylase. *Chem. Biol.* **2002**, *9*, 915−924.

JM049034Y